

# RoTipBot: Robotic Handling of Thin and Flexible Objects using Rotatable Tactile Sensors

Jiaqi Jiang<sup>1,\*</sup>, Xuyang Zhang<sup>1,\*</sup>, Daniel Fernandes Gomes<sup>1</sup>, Thanh-Toan Do<sup>2</sup> and Shan Luo<sup>1</sup>

**Abstract**—This paper introduces RoTipBot, a novel robotic system for handling thin, flexible objects. Different from previous works that are limited to singulating them using suction cups or soft grippers, RoTipBot can grasp and count multiple layers simultaneously, emulating human handling in various environments. Specifically, we develop a novel vision-based tactile sensor named RoTip that can rotate and sense contact information around its tip. Equipped with two RoTip sensors, RoTipBot feeds multiple layers of thin, flexible objects into the centre between its fingers, enabling effective grasping and counting. RoTip’s tactile sensing ensures both fingers maintain good contact with the object, and an adjustment approach is designed to allow the gripper to adapt to changes in the object. Extensive experiments demonstrate the efficacy of the RoTip sensor and the RoTipBot approach. The results show that RoTipBot not only achieves a higher success rate but also grasps and counts multiple layers simultaneously – capabilities not possible with previous methods. Furthermore, RoTipBot operates up to three times faster than state-of-the-art methods. The success of RoTipBot paves the way for future research in object manipulation using mobilised tactile sensors. All the materials used in this paper are available at <https://sites.google.com/view/rotipbot>.

**Index Terms**—Tactile sensing, tactile robotics, robotic handling, deformable object manipulation.

## I. INTRODUCTION

**T**HIN, flexible objects are common in our daily lives, e.g., plastic wrap in kitchens, printer paper in offices and delicate lab gloves. Handling these objects is becoming increasingly important for assistive robots, driven by the growing demand for their use in household and everyday settings. For example, assistive robots need to be able to turn pages with precision to help the elderly read and use plastic wrap to store food. Therefore, the development of robotic systems capable of handling these thin, flexible materials with precision is essential for the next generation of assistive robots.

However, thin and flexible objects, characterised by their relatively small thickness compared to their length and width, and their ability to bend or flex without breaking, present two primary challenges for assistive robots. First, their thinness often results in layers that stack over each other, making the states beneath the top layer difficult to discern with a camera,

Manuscript received 31 January 2024; This work was supported by the EPSRC project “ViTac: Visual-Tactile Synergy for Handling Flexible Materials” (EP/T033517/2).

<sup>1</sup>Jiaqi Jiang, Xuyang Zhang, Daniel Fernandes Gomes and Shan Luo are with the Department of Engineering, King’s College London, London WC2R 2LS, U.K. Emails: {jiaqi.l.jiang, xuyang.zhang, shan.luo}@kcl.ac.uk.

<sup>2</sup>T.-T. Do is with Department of Data Science and AI, Monash University, Clayton, VIC 3800, Australia. E-mail: toan.do@monash.edu.

\* represents equal contributions.

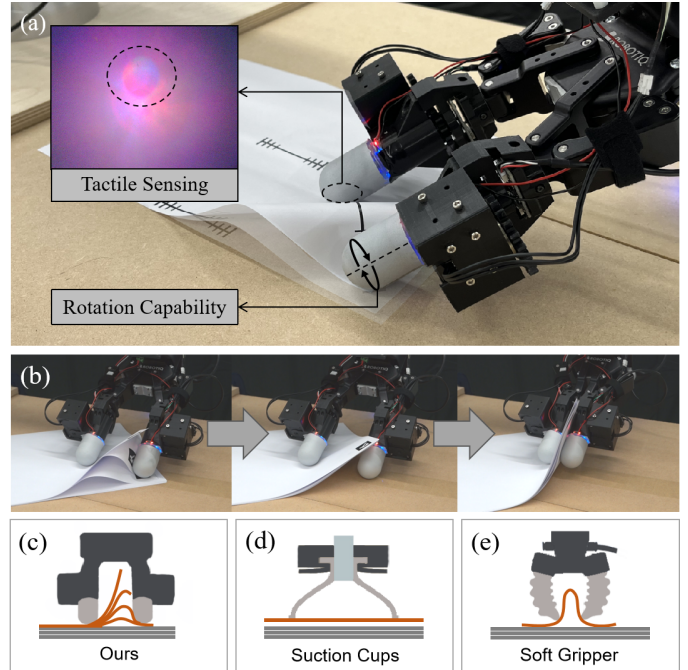


Fig. 1: (a) A demonstration of RoTipBot. The tactile sensors ensure good contact with objects, while the rotation capability feeds multiple layers of thin, flexible objects into the centre for grasping and counting. Different transparencies of the paper represent states at different time steps. (b) Snapshots of the feeding process for multiple print papers. (c-e) Sketches comparing RoTipBot to approaches based on suction cups and soft grippers. RoTipBot can grasp and count multiple layers, whereas the other methods cannot.

resulting into incomplete and noisy perception [1], [2]. On the other hand, the tendency of such objects to deform may require dexterity and compliance in robotic grippers [2]–[4].

Existing approaches for grasping thin, flexible objects often bypass these two challenges. Methods typically assume objects are in known positions [5], or rely on costly force/torque sensors to compensate for the noise in visual perception [1], significantly increasing the overall cost. For the second challenge, specialised mechanisms like suction [6], [7] and two-finger soft grippers [1], [4], [8] are used. However, these mechanisms allow only one page to be grasped at a time, limiting efficiency. Suction cups struggle with air gaps between sheets, preventing effective vacuum seals, while two-finger soft grippers [1], [4], [8] lack the dexterity for continuous picking and holding multiple sheets securely.

To address the above challenges in handling thin and flexible objects, in this paper we propose a novel robotic approach named *RoTipBot* that uses rotatable tactile sensors to sense the contacts with these objects and to feed multiple layers of these objects into the centre for grasping and counting.

We develop a new vision-based tactile sensor named *RoTip*, which can sense the entire fingertip area and actively rotate its body. As shown in Fig. 1-(a), *RoTip*'s sensing capability mitigates visual perception noise and ensures good contact with objects. Its rotational capability adds an extra Degree of Freedom, enhancing dexterity in handling thin and flexible objects. A segmentation and projection model is developed to obtain contact areas and surface planes to guide grasping. As shown in Fig. 1-(b), the passive finger of *RoTipBot* holds the object while the active finger rotates to feed multiple layers into the centre. To adapt to the changes in stacked thickness, the fingers continuously adjust their pose to maintain contact and ensure accurate control when grasping multiple layers.

We conducted extensive experiments to evaluate the *RoTip* sensor and *RoTipBot* approach. The *RoTip* sensor can accurately estimate contact surface planes with an average error of  $1.51^\circ$ . The *RoTipBot* outperforms state-of-the-art methods [1], [8] in overall success rate and operates up to  $3\times$  faster. More importantly, it enables the grasping of multiple layers for the first time. The success of *RoTipBot* paves the way for future research in object manipulation using mobilised tactile sensors.

Our contributions can be summarised as follows:

- We introduce *RoTipBot*, a novel robot for handling thin and flexible objects that can grasp and count them for the first time.
- The *RoTip* sensors in *RoTipBot* can sense contacts across the entire fingertip surface, with an additional motor enhancing dexterity by actively rotating the sensor to slide along the object's surface.
- We conducted comprehensive experiments to evaluate *RoTipBot*, demonstrating its ability to grasp and count multiple layers of thin and flexible objects, with high success rates and efficiency.

The rest of this paper is structured as follows. Section II reviews the related works and Section III introduces the design of *RoTip* and its perception capability; Section IV details *RoTipBot* for thin and flexible object handling; Section V analyses the experimental results; Finally, Section VI discusses the work and Section VII concludes the paper.

## II. RELATED WORKS

### A. Vision-based Tactile Sensors

In recent years, many vision-based tactile sensors have been developed, primarily classified into two main categories: the *GelSight* family [9], which processes raw images and employs photometric stereo for shape reconstruction; the *TacTip* family [10], which estimates contact by tracking pin displacement. Unlike *TacTip*, which is limited by pin resolution, *GelSight* offers superior resolution and detailed texture information [11]. Our *RoTip* sensor belongs to the *GelSight* family.

The first *GelSight* prototype was developed in 2009 by Johnson and Adelson [12]. Following that, a set of subsequent developments were built with different focuses, such as enhanced lighting setups of *GelSight-2017* [9] and *GelSlim 3.0* [13], sensor reproducibility of *DIGIT* [14], and a compact shape for robot fingers of [15]. While previous *GelSight* tactile sensors capture high-resolution tactile images, their limited sensing

area poses challenges for complex robotic manipulation. To address this, recent works have introduced finger-shaped tactile sensors, such as *GelTip* [16], *OmniTact* [17], *Insight* [18] and *GelSight360* [19]. These sensors can be mounted on off-the-shelf parallel grippers to enhance manipulation tasks with tactile sensing.

However, these setups possess limited degrees of freedom, decoupling tactile sensing from robotic dexterity. Hence, several studies have explored the integration of rotational movement into tactile sensors to enhance functionality. *TouchRoller* [20] was proposed to rapidly reconstruct large contact surfaces through surface rotation, while *TacRot* [21] utilises a rotatable surface to facilitate in-hand object manipulation. The tactile-reactive roller grasper (TRRG) [22] integrates compliant, steerable cylindrical fingertips for improved manipulation. Despite these advancements, they only perceive the inner side of the fingertip, preventing interaction modes such as pressing or poking. To our best knowledge, *RoTip* is the first tactile sensor that can sense the entire fingertip area and actively rotate its finger body. These two capabilities are crucial for addressing the challenges of incomplete visual perception and the need for dexterity in handling thin and flexible objects.

### B. Thin and Flexible Object Grasping

Deformable object manipulation has been a growing research area with various applications, such as assembling cables in factories [23]–[26], assisted dressing and laundry folding [27]–[30] and food production [31], [32]. These tasks mainly rely on visual perception [23], [28], [32]–[34]. However, the specific challenge of manipulating thin and flexible objects remains relatively unexplored. The small thickness of these objects compared to their length and width and their stacked layers complicates visual perception and grasping.

Recent approaches to manipulating thin and flexible objects focus on the control design. Several studies achieve thin object grasping via pre-grasp motions such as sliding [35] and scooping [36], [37]. In [35], thin objects are slid to the table edge and grasped from the side. In [36], stable grasps of thin objects are achieved through scooping actions. In [37], a prying strategy is proposed to tilt a thin object like a card to create clearance beneath it for a stable pinch grasp. Similarly, in [38], an underactuated crawler is used to tilt thin objects for pinch grasps.

Some other studies focus on specialised grasping mechanisms. Suction cups in [6], [7] are investigated for handling thin, flexible objects due to their non-damaging, evenly distributed gripping force and simple grasp procedure. Specifically, in [7], a two-finger gripper integrated with a suction cup is developed for grasping different kinds of objects including thin, flexible ones. However, the effectiveness of the suction mechanism is limited by the need for a smooth surface to create a vacuum seal. When attempting to pick up multiple sheets, air gaps between them prevent the formation of an even vacuum seal, resulting in ineffective or incomplete picks.

Another mechanism used for grasping delicate materials is the soft gripper. As discussed in [4], the three-axis compliance

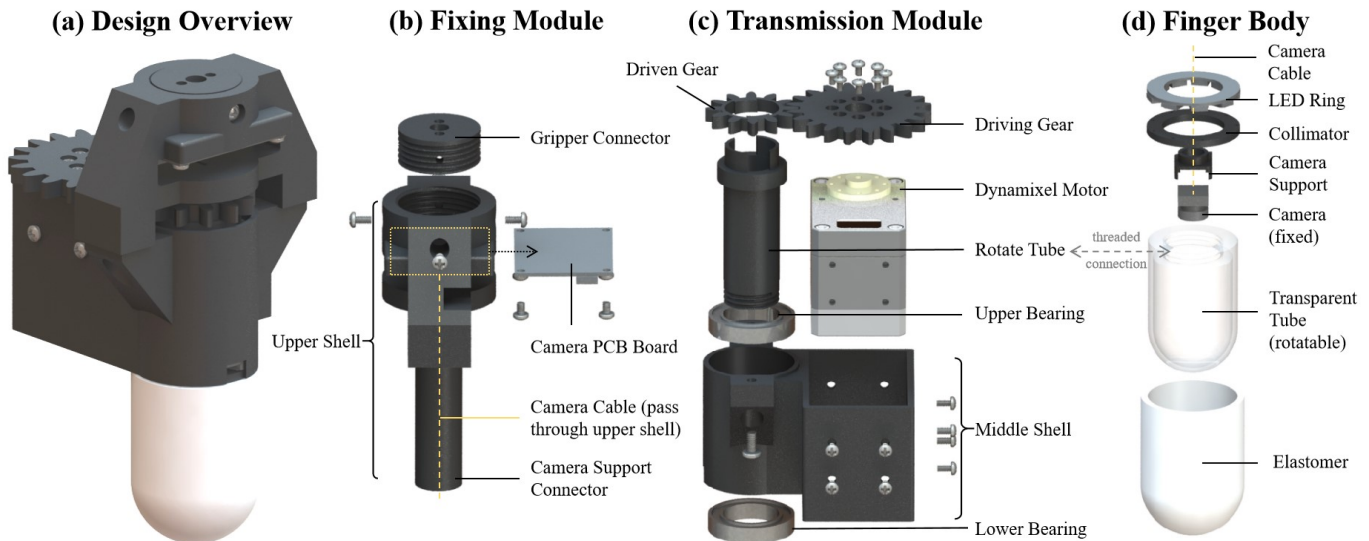


Fig. 2: **From Left to Right:** (a) **Design overview** of the RoTip sensor, and the exploded view of RoTip’s three modules: (b) **fixing module** that serves as the structural backbone, ensuring stability and interconnection among sensor components; (c) **transmission module** that facilitates rotational movement, enabling dynamic functionality; and (d) **finger body** that constitutes the tactile interface, providing the tactile sensing capabilities.

of a soft gripper provides unique benefits for grasping thin, flexible objects. In [8], a two-finger soft gripper is used to deform an object for a pinch grasp, but this approach requires knowledge of physical properties, such as friction, to model object deformation dynamics. Building on this, FlipBot introduced in [1] uses a two-finger soft gripper with a force/torque sensor to singulate and grasp thin and flexible objects by integrating exteroceptive and proprioceptive perceptions. However, it uses a force/torque sensor that only provides contact information at a single point, and can only grasp one page at a time, limiting its efficiency. In contrast, our RoTipBot offers rich distributed contact information using vision-based tactile sensing, and its rotation capability enables the grasping of multiple thin, flexible objects simultaneously. Another related work, [5], leverages tactile feedback to handle thin and flexible objects like paper, but simplifies the problem by placing paper on the edge of the table for easy pickup, bypassing the challenge of grasping from the table surface. Our RoTipBot addresses these issues effectively, proving its capability in these complex tasks.

### III. THE ROTIP SENSOR

In this section, we introduce RoTip, a novel vision-based tactile sensor that can sense the entire fingertip area and rotate along the vertical axis, as shown in Fig. 2. The sensor can be easily attached to different commercial grippers, such as the Robotiq-2f Gripper, as shown in Fig. 1-(a). We provide detailed descriptions of both the hardware and firmware to enable the research community to reproduce the sensor. A GitHub repository containing all necessary files has been prepared for interested readers.

#### A. Sensor Design

The proposed RoTip sensor comprises three primary modules: the fixing module, the transmission module and the

finger body, as shown in Fig. 2-(b), (c) and (d), respectively. The fixing module is used for secure attachment and precise positioning of the transmission module and the finger body, ensuring stability during operation. Meanwhile, the transmission module is used to drive the rotational motion, enabling dynamic functionality. Lastly, the finger body serves as the tactile interface, providing the sensor’s tactile perception capabilities. Further insights into these three modules are elaborated below:

1) *Fixing module:* The fixing module of the RoTip sensor is designed for connecting and bolstering other components of the sensor, as shown in Fig 2-(b). It features a gripper connector, allowing for easy and secure attachment to a diverse range of robotic grippers. Both threaded mechanisms and screws are used to link the gripper connector and upper shell, so as to support forces and torques during interactions with objects. Moreover, the module incorporates a dedicated support structure tailored for the Printed Circuit Board (PCB) of a camera, ensuring the camera’s stability. Additionally, the bottom section of the fixing module is designed for camera connection, ensuring that the camera maintains its position even when the finger body rotates. To protect the camera’s functionality, the camera cable is neatly channelled through a tube within the fixing module.

2) *Transmission module:* The transmission module in our RoTip sensor features a gear transmission mechanism as shown in Fig. 2-(c). The Degree of Freedom for each finger is managed by a Robotis Dynamixel XM430-W350 actuator<sup>1</sup>, capable of executing different control modes: precise position control mode from 0° to 360° and velocity control mode for endless turns. To optimise performance, a transmission ratio of 5:3 was chosen to balance torque and speed, ensuring both efficient and responsive movements. This ratio not only enhances operational smoothness but also mitigates gear collision risks when the gripper is closed. Moreover, two 6803-

<sup>1</sup><https://robotis.co.uk/dynamixel-xm430-w350-r.html>



Fig. 3: (a) and (b) represent RoTip sensor with a **hemisphere tip** and a **flat tip**, respectively. In the first two rows, the transparent support shells, the coated elastomer, and the corresponding tactile images are presented from left to right. Notably, sparking points in the centre of the tactile image are discernible due to the intense reflection from the flat tip. (c) showcases the tactile readings captured as the RoTip sensor with a hemisphere tip interacts with a bolt, a nut, and a USB cable.

2RS ball bearings, each sized at  $17mm \times 26mm \times 5mm$ , are utilised in the design to facilitate smooth rotational movement and provide stability to the moving parts of the system. For software integration, we utilise the DynamixelSDK, which is programmed in Python. This choice facilitates seamless integration with various deep-learning approaches, enhancing the sensor’s overall adaptability and versatility.

3) *Finger body*: The finger body serves as a tactile interface, resembling a fingertip, crucial for interacting with the environment. Following the design principles of our previous vision-based tactile sensor GelTip [16], our RoTip incorporates an elastomer with an opaque coating layer to enhance tactile feedback, along with a rigid transparent shell that provides structural support to the elastomer. To accommodate the camera, we set the radius of the rigid shell at 28 mm with a thickness of 2 mm to ensure sufficient hardness. Threaded mounting was employed to not only enhance the sensor’s stability but also facilitate replicability. This modular design allows for easy interchangeability of finger bodies, including alternative shapes like the flat-tipped variant shown in Fig. 3-(b) instead of the hemisphere tip.

To achieve uniform illumination, we designed a PCB with multiple LEDs arranged in a circular pattern as shown in Fig. 2-(d). Following [18], we incorporated a collimator over the LED PCB. Additionally, a diffuser was used to mitigate lighting sparks and enhance contrast and uniformity of tactile imprints, as suggested in [15]. The combination of photometric effects and structured lighting empowers the camera to precisely detect the deformations of the elastomer when it comes into physical contact with objects, such as the thread of a bolt, as illustrated in Fig. 3-(c).

**Remark:** For effective grasping of thin and flexible objects, it is essential that the RoTip sensors mounted on the gripper make contact during closure. To this end, the finger radius must be larger than that of any other component, including

the transmission device and the shell.

## B. Sensor Fabrication

In the fabrication of RoTip sensors, several components, such as the camera and LED PCB, are commercially available. For instance, we utilise an OV5640 camera<sup>2</sup> with a 160-degree field of view to capture tactile images. This camera is fitted into a compact camera holder, which allows for stable placement and orientation adjustment. The LED PCB is sourced from a specialised manufacturer, and detailed specifications are available on our website. However, for other critical parts such as the finger body, we have to manually design and create custom moulds and fabricate its rigid shell and elastomer.

1) *Transparent fingertip shell*: We adopt a fabrication process utilising Stereolithography (SLA) 3D printing, in contrast to our previous approach in [16] that used a standard transparent test tube. This new method involves creating the shell with clear resin, which is subsequently refined through surface polishing and lacquer coating [39], resulting in a remarkably transparent shell as shown in Fig. 3. Additionally, we have adopted threading for assembling the fingertip shell, which enhances stability and eliminates the complexities associated with using screws. It is important to note that applying a lacquer coating slightly increases the thickness of the thread. As a result, the component designated for mounting the rigid shell needs to be adjusted to accommodate this slight change in dimension.

2) *Elastomer*: We use the same materials in our previous work [16], i.e., XP-565 from Silicones, Inc. (High Point, NC, USA) and Slacker from Smooth-on Company. After extensive experiments we found the best ratios to be 1:15:15, i.e., 1 gram of XP-565 part A, 15 grams of XP-565 part B and 15 grams of the Slacker. This amount of mixture is sufficient to fabricate four sensor membranes. The elastomer is fabricated through moulding with a two-piece mould, as shown in Fig. 4. To fabricate the rigid parts, we take advantage of 3D printing technology, specifically SLA printing, due to its ability to produce much smoother mould surfaces, significantly impacts the quality of the elastomer. A thorough polishing step is also necessary to eliminate the layer lines from the 3D printing process.

The exterior of the elastomer is coated with an opaque reflective material aimed to contain and intensify the lighting within the shell. Aluminium powder with reflective pigment was used for coatings, as suggested in [9]. Specifically, the optimal ratio for the coating mixture is 1:15:4:4:10, i.e., 1 gram of XP-565 part A, 15 grams of XP-565 part B, 4 grams of aluminium powder, 4 grams of Silver Cast Magic® from the Smooth-on Company, and 10 grams of NOVOCS Matte Solvent. Then the cured silicone base was dipped into this mixture to form the opaque reflective coating layer. The acquired coating has proven to be durable and reliable under high contact forces. Figure 3-(c) demonstrates high-resolution and clear tactile images captured during contact with various objects, e.g., a bolt, a nut and a USB cable.

<sup>2</sup><https://www.waveshare.com/ov5640-camera-board-a.htm>

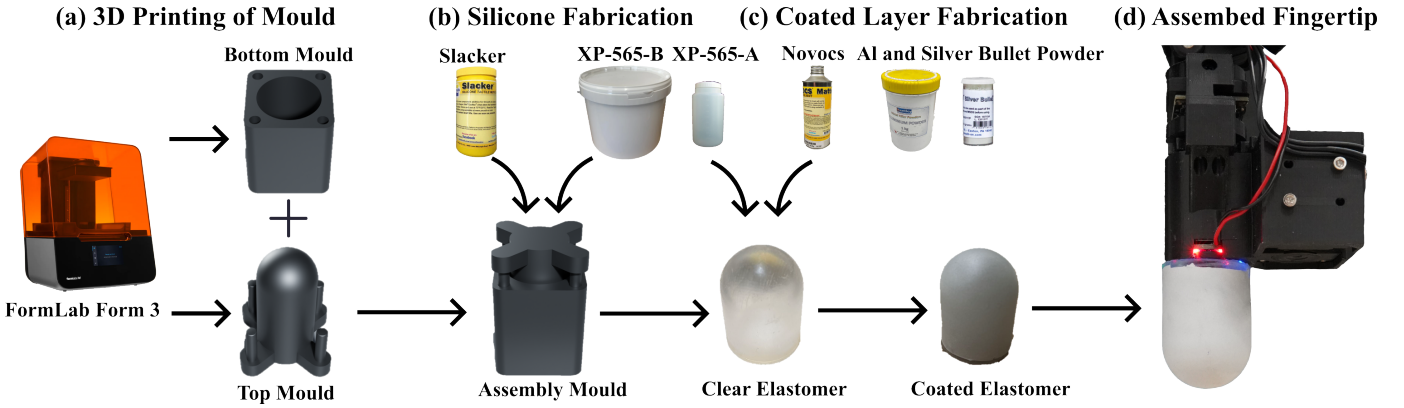


Fig. 4: Fabrication of RoTip’s fingertip. There are three main steps for this fabrication process: (a) 3D printing of moulds using the FormLab Form 3 3D printer; (b) Silicone fabrication through mixing XP-565 Silicone with the slacker to obtain the clear elastomer; (c) Coated layer fabrication through mixing XP565 with NOVOCs solvent, aluminium powder, and Silver Bullet powder; and finally (d) Assembled fingertip.

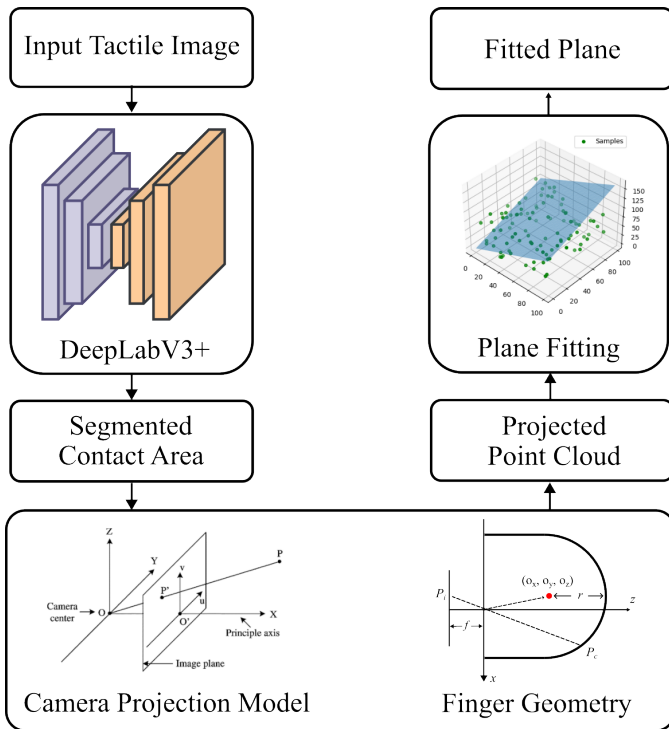


Fig. 5: Pipeline for tactile perception. Given a tactile image as input, a fine-tuned DeepLab v3+ [40] network is used to segment the contact area of the RoTip sensor. Then, the contour of the contact area can be obtained based on the camera projection model and the finger geometry. Finally, a RANSAC-based plane fitting approach is used to derive the parameters of the contact plane.

### C. RoTip Contact Perception and Kinematic Model

In this subsection, we will introduce the contact perception pipeline for the RoTip sensor. As shown in Fig. 5, the captured tactile image is first fed to a fine-tuned DeepLab v3+ network [40] to segment the contact area. Following this, the camera’s projection model is used to reconstruct the point cloud representing the boundary of the contact area. Given the reconstructed point cloud, a RANSAC-based plane-fitting approach is used to derive the parameters of the plane where contact occurs. In addition to the contact perception, the kinematic model of the RoTip is introduced to facilitate the thin and flexible object manipulation detailed in Sec. IV.

1) *Contact Segmentation*: The contact area segmentation is treated as a semantic segmentation problem that predicts each input image pixel into one of two semantic classes: (a) background and (b) contact area. To this end, we use the Deeplab v3+ model [40] to segment the contact areas in tactile images considering its good accuracy and computational efficiency.

For data collection, we employed a robotic arm equipped with RoTip sensors to interact with two different kinds of materials to represent thin and flexible objects, i.e., printer paper with a smooth surface and fabrics with varied textures, at various angles. A total of 392 tactile images with annotated Ground Truth (GT) masks were initially gathered from these materials, with the data collection setup illustrated in Fig. 15. To enhance the diversity of the dataset, additional augmentation techniques such as flipping, rotation, cropping, and contrast adjustments were applied, expanding the dataset to comprise 4,000 tactile images. Then this dataset was split into 70:30 for training and testing. Key hyperparameters for the model include an SGD optimiser with a learning rate of  $1e-5$ , momentum of 0.9, and weight decay of  $5e-4$ , and a vanilla cross-entropy loss was used for training.

Dilated Residual Networks (DRN) [41] and Residual Networks (ResNet) [42] architectures were evaluated as backbones at three different input resolutions: 512, 256, and 128. The performance of each network configuration was measured using two metrics: mIoU (mean Intersection over Union) for the accuracy of segmentation tasks, and frequency representing the processing speed of the network (frames per second). All the models were tested with an Nvidia RTX-3090 graphic card for a fair comparison. As shown in Table I, there is a trade-off between accuracy and speed. Generally, as the input size decreases, the frequency generally increases, which suggests faster processing but potentially at the cost of reduced segmentation accuracy. However, ResNet-50 with an input size of 256 achieves a good balance between the two, with a high mIoU of 96.92% as well as a high frequency of 173.74 Hz. Therefore, we selected ResNet-50 with a  $256 \times 256$  input as the backbone of the network.

Compared to the traditional image processing approach we used in the GelTip sensor [16], [43] for contact detection, the method using the above deep neural network is more

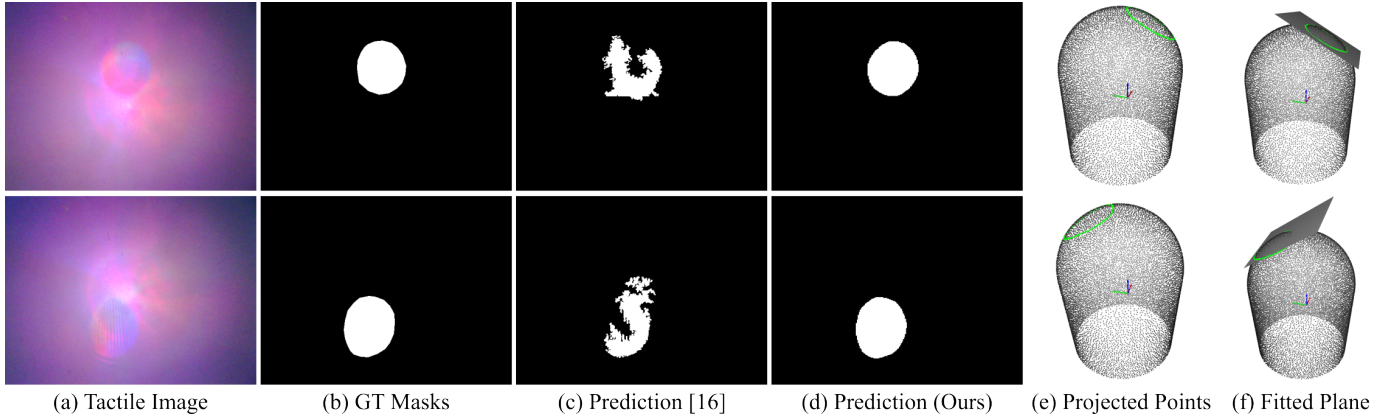


Fig. 6: Contact segmentation and plane fitting of the contact on the RoTip tactile sensor. From left to right: (a) Two examples of raw tactile images on two rows; (b) Ground Truth (GT) masks of the contact areas; (c) segmentation predictions via image subtraction method used in [16]; (d) segmentation predictions via deep neural networks proposed in this work; (e) visualisation of projected points (green dots) outlining the contact area; and (f) fitted planes during RoTip's contact with a flat surface.

TABLE I: Network architecture for tactile contact segmentation.

Backbone	Input Size	mIoU $\uparrow$ (%)	Frequency $\uparrow$ (Hz)
DRN	512	96.51	44.37
DRN	256	95.61	128.16
DRN	128	90.70	<b>223.81</b>
ResNet-101	512	96.69	64.62
ResNet-101	256	96.80	120.28
ResNet-101	128	95.00	139.48
ResNet-50	512	<u>96.83</u>	79.92
ResNet-50	256	<b>96.92</b>	173.74
ResNet-50	128	95.85	<u>220.84</u>

robust, especially given the slight background changes during the rotation of the finger body. As demonstrated in Fig. 6, the image subtraction method used in GelTip for contact detection produces numerous false positives and negatives. In contrast, our deep neural network approach delivers highly precise segmentation results.

2) *Contact Point Projection*: Based on the general camera projection model [44], the segmented contact areas in pixel coordinates, represented in homogeneous form as  $(u, v, 1)$ , can be converted to normalised image coordinates  $(x_i, y_i, 1)$  for the  $i^{th}$  pixel in the image frame by applying the inverse of the intrinsic matrix  $K$  as follows:

$$\begin{bmatrix} x_i \\ y_i \\ 1 \end{bmatrix} = K^{-1} \cdot \begin{bmatrix} u \\ v \\ 1 \end{bmatrix}, \quad (1)$$

where  $K$  is the camera intrinsic matrix:

$$K = \begin{bmatrix} f_x & 0 & c_x \\ 0 & f_y & c_y \\ 0 & 0 & 1 \end{bmatrix}, \quad (2)$$

in which  $f_x$  and  $f_y$  are focal lengths in  $x$  and  $y$ , respectively;  $c_x$  and  $c_y$  are the offsets in the image frame.

The normalised image position  $(x_i, y_i, 1)$  also represents the direction of the light ray travelling through the sensor membrane, where the contact point  $P_c = (x, y, z)$  on the sensor surface must lie on. Hence, we have

$$[x, y, z] = k * [x_i, y_i, 1], \quad (3)$$

where  $k \in \mathbb{R}$  is a scale parameter.

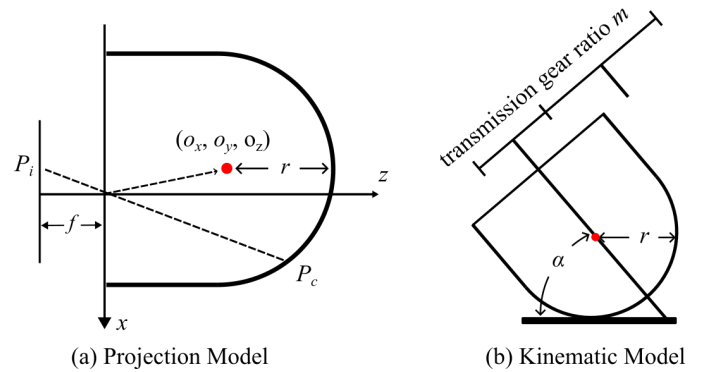


Fig. 7: (a) **Projection model of the camera in the RoTip sensor**. Here,  $f$  represents the focal length, and  $r$  denotes the radius of the hemisphere tip. Points  $P_i$  and  $P_c$  are the projections in the image and camera coordinates, respectively.  $(o_x, o_y, o_z)$  is the offset between the hemisphere centre and the camera optical centre. (b) **Kinematic model of the RoTip sensor**.  $\alpha$  is the rotation angle between the sensor central axis and the contact plane.

As illustrated in Fig. 7-(a), the sensor surface can be modelled as a combination of a hemisphere and an opened cylinder, both sharing the same radius  $r$ . The central axis of the cylinder surface is parallel to the  $z$ -axis. Therefore, the centre point of the hemisphere can be set to  $(o_x, o_y, o_z)$ , where  $o_z$  is the distance from the centre point of the base of the hemisphere to the centre point of the base of the sensor. Then, the location of any point on the sensor surface  $P_c$  can be represented as follows:

$$\begin{cases} (x - o_x)^2 + (y - o_y)^2 + (z - o_z)^2 = r^2 & \text{for } z > o_z \\ (x - o_x)^2 + (y - o_y)^2 = r^2 & \text{for } z \leq o_z \end{cases} \quad (4)$$

By solving Eq. 3 and Eq. 4, we can obtain the contact location on the sensor surface. For example, when the contact position lies on the hemisphere, we will have the following quadratic equation:

$$(x_i^2 + y_i^2 + 1) * k^2 - 2(x_i o_x + y_i o_y + o_z) * k + (o_x^2 + o_y^2 + o_z^2) = r^2, \quad (5)$$

where the solution of  $k$  is equal to the  $z$ -coordinate of  $P_c$ . With the known value of  $k$  and the ray direction  $(x_i, y_i, 1)$ , the contact location can be obtained via Eq. 3.

3) *Contact Plane Estimation*: Given the estimated boundary of contact areas, a RANSAC-based plane fitting method is used to estimate the surface normal of the contact plane in 3D space. By identifying the contact plane, the robot could adjust its end-effector pose for optimal contact. The process begins by randomly selecting three points and using Singular Value Decomposition (SVD) to initialise the plane parameters [45]. It then detects all points belonging to the calculated plane within a given threshold. This procedure is repeated  $n$  ( $= 100$  in our case) times for efficiency. During each iteration, the plane parameters are updated if the new result is better than the previous best one. Examples of the fitted planes are shown in Fig. 6-(f).

To achieve accurate tactile perception with RoTip sensors, two key components need to be calibrated: the camera intrinsic matrix, and the extrinsic offset  $(o_x, o_y, o_z)$  as shown in Fig. 7. Similar to the method in [22], we use a 7x8 checkerboard mounted on a board to get the sensor intrinsic with ROS calibration tools. During camera calibration, multiple sensor images are collected with different checkerboard poses to compute the camera intrinsic matrix  $K$ . Next, we calibrate extrinsic offsets  $o_x$  and  $o_y$  using tactile images from vertical contact with a flat surface, ensuring the contact area is centred on the fingertip. This step is treated as an optimisation problem aiming to minimise the distance between the predicted contact region's centre and the fingertip's top. Finally, we calibrate the offset  $o_z$  along the camera's  $z$ -axis by minimising the error between the predicted contact plane and the actual contact plane, using the tactile images collected at tilted angles, specifically  $45^\circ$  and  $-45^\circ$ .

**Remark:** We chose not to adopt an end-to-end approach for contact surface prediction because it would require training a model for each individual RoTip sensor. Instead, by calibrating only the offset parameters  $(o_x, o_y, o_z)$  for each sensor, our approach simplifies the calibration process and enhances the model's generalisation across RoTip sensors with varying installation errors.

4) *Kinematic model of the RoTip*: The proposed RoTip's distinctive capability includes self-actuated rotation, making it crucial to understand its kinematic model. As shown in Fig. 7-(b), we assume the contact angle between the finger and the object is  $\alpha$ . Then the effective rotation radius is approximately equal to  $r * \cos(\alpha)$ . Considering the transmission ratio  $m$ , the movement speed  $v$  of the contact area is given by:

$$v = \omega * m * r * \cos \alpha \quad (6)$$

where  $\omega$  is the rotation speed of the actuator.

5) *Discussion on the Need of Force Estimation*: Previous studies such as GelSight [9], Insight [18], and AllSight [39] employed neural networks to predict contact forces. Inspired by these achievements, we attempted to implement force estimation with our RoTip sensor, particularly when it comes into contact with thin and flexible objects. However, we encountered a significant challenge: there were minimal observable changes in the sensor's output, both visually and through the segmentation model, when the applied force was below 3N.

This lack of observable change can be attributed to the nature of the contact surface. In previous studies that involved a small rigid indenter, even a small applied force could lead to significant changes in the tactile image. This is because the small indenter concentrates the force onto a tiny area, creating high pressure and producing a clear, measurable deformation in the sensor's surface. In contrast, when interacting with a flat surface of thin and flexible objects, the same level of force is distributed across a larger area, making changes much less noticeable and difficult to quantify.

Given these findings, pursuing force estimation for the RoTip sensors in scenarios involving interaction with flat surfaces of thin and flexible materials was deemed impractical. The subtle deformations under low force conditions would not provide reliable data for accurate force prediction. This conclusion also applies to other vision-based tactile sensors such as GelSight [9], GelTip [16], Insight [18] and AllSight [39], where thin and flexible objects diffuse applied forces over a broader surface area. Instead, we chose to leverage the force signals from the UR5e robotic arm to achieve real-time feedback control during contact with thin and flexible objects. This approach allows us to maintain effective manipulation and interaction without relying on the RoTip sensor for precise force measurement, thereby simplifying the system and focusing on its strengths in tactile perception and dynamic adjustment.

#### IV. THIN AND FLEXIBLE OBJECT GRASPING

In this section, we introduce RoTipBot, a system using the RoTip rotatable tactile sensors to grasp multiple thin, flexible objects simultaneously. RoTipBot uses a two-finger gripper to handle thin and flexible objects: one **passive** finger holds the object, while the other **active** finger rotates to feed multiple sheets into the centre between the two fingers, allowing them to be grasped all at once. This method prevents pinching the paper from the same side, thereby avoiding potential damage and ensuring a more secure grasp. Though in this work we demonstrate the RoTipBot with a two-finger gripper, it is generalisable to a robotic hand with more than two fingers.

First, we present the setup of hardware and system configuration. Then, we perform a force analysis to identify the optimal location that requires minimal force to squeeze and feed thin, flexible objects. Real-world grasping poses are obtained using an RGB-D camera, providing precise and reliable data for the manipulation task. Following that, we propose a tactile-based adjustment method based on RoTip's perception capability to adjust the pose of the end-effector, ensuring grasp stability. Finally, we introduce a continuous adjustment method to address the changes in stacked thickness during the feeding process of multiple layers of the object for grasping. This method ensures consistent grasping performance despite variations in object thickness.

##### A. Hardware Setup

As shown in Fig. 8-(a), our robot setup consists of a 6-DOF UR5e robot<sup>3</sup>, a Robotiq 2F-85 adaptive gripper<sup>4</sup>, and

<sup>3</sup><https://www.universal-robots.com/products/ur5-robot/>

<sup>4</sup><https://robotiq.com/products/2f85-140-adaptive-robot-gripper>

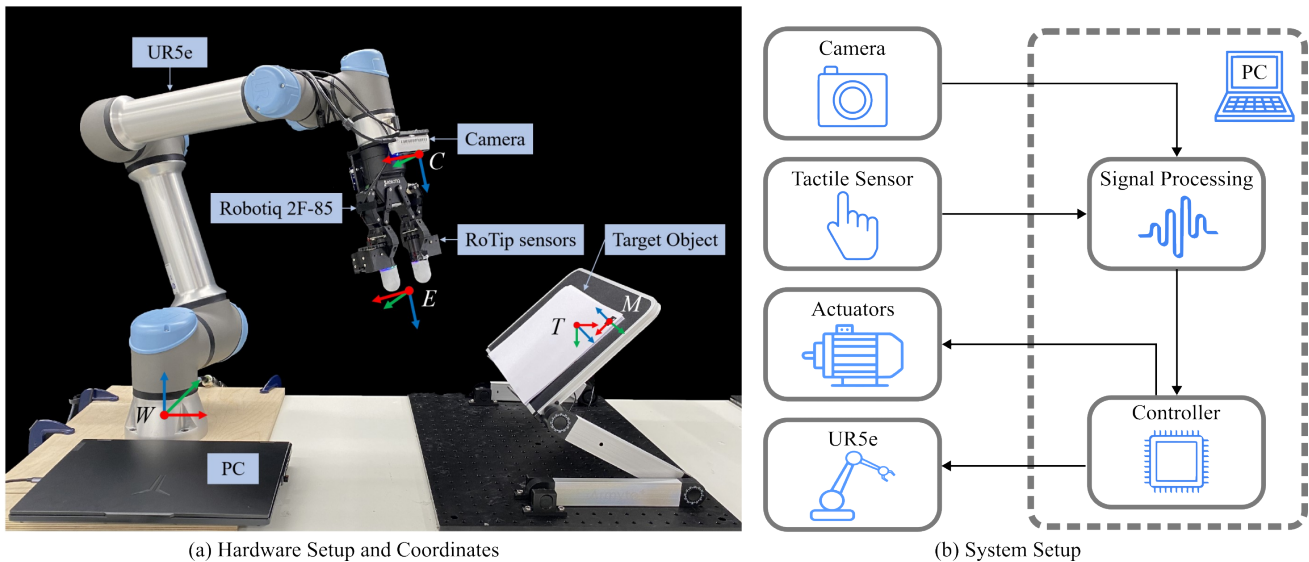


Fig. 8: **(a) Hardware Setup and Coordinates.** The hardware setup consists of a 6-DOF UR5e robotic arm, a Robotiq 2F-85 gripper, an Intel RealSense D435 RGB-D camera, and a laptop stand for holding the printer papers or other thin and flexible objects. The fingertips of the Robotiq gripper are replaced with two RoTip sensors.  $W$  and  $E$  represent the world coordinate that is located at the base of UR5e and the end-effector coordinate, respectively.  $C$  and  $M$  represent the camera coordinate and the marker coordinate, respectively.  $T$  is the target coordinate related to the marker coordinate and used to direct the movement of the end-effector. **(b) System setup.** The PC plays two roles: processing the signals obtained from the camera and RoTip sensors, and utilising the processed signal to control the actuators and UR5e robotic arm for thin and flexible object handling.

an Intel RealSense D435 RGB-D camera<sup>5</sup>. The fingertips of the Robotiq gripper are replaced with two RoTip sensors. All the above devices are connected to a laptop equipped with an Nvidia RTX 4060 GPU. The setup of the robotic system is depicted in Fig. 8-(b). In this configuration, the laptop is responsible for managing the signal processing of the RealSense camera and the RoTip sensors. It processes visual and tactile feedback to generate control commands for the Dynamixel motors within the RoTip sensors, as well as the UR5e robotic arm for thin and flexible object handling. Furthermore, for evaluating the grasp in various poses, we utilise an adjustable stand mounted to the test board on the table. This stand is designed to hold the thin and flexible object intended for grasping, enabling consistent and reliable experimentation.

In this work, we establish five distinct coordinate systems, using the base of the UR5e robotic arm as the origin for the world coordinate system, denoted as  $W$ . The end-effector coordinate, denoted as  $E$ , is initially positioned at the centre of the two RoTip sensors and can be dynamically tracked via the UR5e ROS driver. The camera coordinate system,  $C$ , is located at the RGB component of the RealSense camera. To streamline the calibration process between the camera and the end-effector, a specialised mounting component is designed, ensuring only translational offsets exist between these two coordinates. Additionally, we identify the corner of the thin and flexible object, marked by an ArUco marker, as the marker coordinate system, represented as  $M$ . The final target coordinate for the grasping action, denoted as  $T$ , is established to direct the movement of the end-effector. The transformation  $T_M^T$  from  $T$  to  $M$  is predefined to make the line connecting the two fingers parallel to the angle bisector of the object's corner.

## B. Vision-Guided Grasp Pose Estimation

In this subsection, we first conduct theoretical force analysis to identify the optimal location for squeezing and feeding thin and flexible objects. Through the analysis, we identify the corners of these objects as the optimal location. Following this, we estimate the real-world grasping poses with an RGB-D camera. To facilitate corner detection, we employ ArUco markers, streamlining the process and allowing us to concentrate on the primary challenges addressed by the proposed RoTip sensors: overcoming incomplete visual perception of stacked layers and enhancing dexterity in handling thin and flexible objects.

1) *Grasp Location Analysis:* Unlike rigid objects, which can often be grasped at their centres [46] or top surfaces [47], theoretical studies have yet to determine the optimal grasping positions for thin and flexible objects due to their minimal thickness and complex kinematics. Therefore, it is crucial to identify the optimal locations for squeezing and feeding these objects, prioritising two key factors: maximising handling speed and minimising the required force.

**Maximising handling speed:** Handling speed is directly influenced by the speed at which thin and flexible objects can be fed. Given that the RoTip sensor rotates at a constant speed, a shorter path will result in faster feeding. Therefore, it is evident that squeezing from the corners significantly reduces the movement distance of the fingers compared to squeezing from the middle or other positions, resulting in quicker handling.

**Minimising force required for handling:** It is critical to minimise the force during handling thin and flexible objects to prevent potential damage to the object while securing manipulation. We employ beam theory [48] to analyse the force involved in the deformation of such objects when they are manipulated by our proposed RoTip sensors. This sec-

<sup>5</sup><https://www.intelrealsense.com/depth-camera-d435/>

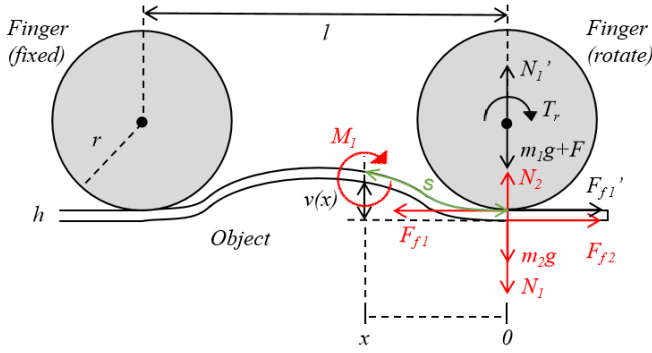


Fig. 9: Theoretical force analysis of squeezing the thin and flexible object with our RoTip sensors (cross section view). The black arrows and red arrows represent the forces and torques applied to the finger and the object, respectively.

tion details the theoretical force analysis when the object is squeezed into a curved shape, as illustrated in Fig. 9.

To prevent relative sliding between the finger and the object, according to Coulomb's law and as shown in Fig. 9 for the rotating finger on the right, the friction between the finger and the object  $F_{f1}'$  must be less than the product of static friction coefficient  $\mu_{s1}$  and the normal forces generated between the object and the finger  $N_1'$ , i.e.,

$$F_{f1}' \leq \mu_{s1} N_1' \quad (7)$$

Also, when the finger maintains contact with the object, the sum of the forces acting on the fingers must equal zero, i.e.,

$$\begin{cases} N_1' = m_1g + F \\ F_{f1}' = T_r/r \end{cases} \quad (8)$$

where  $m_1g$ ,  $F$ ,  $T_r$  and  $r$  are the gravity, the vertical force, the torque applied to the finger and the finger radius, respectively.

On the other hand, to ensure that the object can continue to bend and arch, the friction between the finger and the object  $F_{f1}$  applied to the object must be greater than the sum of the friction between the object and the table  $F_{f2}$  and the force resulting from the rotation of the finger, i.e.,

$$F_{f1} \geq F_{f2} + \frac{M_1}{v(x)} \quad (9)$$

where  $M_1$  and  $v(x)$  represent the bending moment and the vertical deflection at position  $x$ , respectively; From Fig. 9, we know that:

$$F_{f2} = \mu_{k2} N_2 = \mu_{k2}(m_2g + N_1) = \mu_{k2}(m_2g + m_1g + F) \quad (10)$$

where  $\mu_{k2}$  is the dynamic friction coefficient of  $F_{f2}$  and  $m_2g$  is the gravity of the object.

According to beam theory [48], there are two cases for calculating  $M_1$ : small deflection and large deflection. These cases are defined based on whether the deflection  $v(x)$  reaches one-tenth of the distance  $l$  between the two fingers:

$$M_1 = \begin{cases} EI_z v''(x), & \text{when } v(x) \leq \frac{l}{10} \\ EI_z \frac{ds}{d\kappa}, & \text{when } v(x) > \frac{l}{10} \end{cases} \quad (11)$$

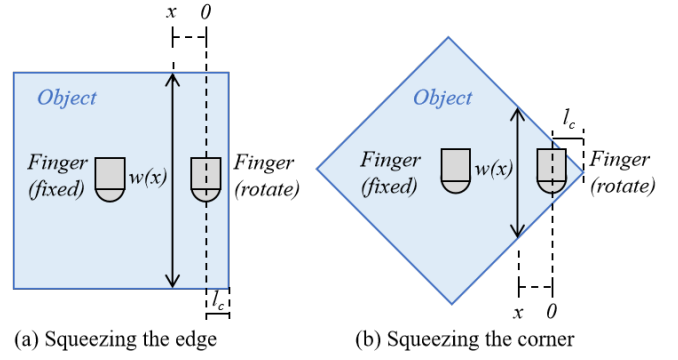


Fig. 10: Finger squeezing at (a) the edge and (b) the corner of the object.

where  $E$  is the elastic modulus,  $v''(x)$  is the curvature of the object (the second derivative of  $v(x)$ ),  $s$  is the arc length along the deflected object between position 0 end and position  $x$  as shown in Fig. 9, and  $\kappa$  is the slope at position  $x$ ;  $I_z$  is the moment of inertia of the object:

$$I_z = \int_0^l \frac{w(x)h^3}{12} dx \quad (12)$$

where  $w(x)$  is the width of the contact edge at position  $x$ , as shown in Fig. 10, and  $h$  is the thickness of each layer.

From Eqs. 9-12, we can find that the minimum force required to squeeze the thin and flexible object has a positive correlation with the ratio  $\frac{M_1}{v(x)}$ ; Considering the same bending curve of the object at different squeeze locations, the deflection  $v(x)$  and the curvature  $v''(x)$  or  $\frac{ds}{d\kappa}$  of the object remain the same. Hence, the optimal location for grasping is where  $M_1$  is minimised, which occurs at the corners of the object due to the minimal  $\int_0^l w(x)dx$  based on Eq. 11-12, and as shown in Fig. 10. Therefore, squeezing at the corners of the object results in minimal force for effective handling.

2) *Grasp Pose Estimation*: After determining that the corners are the optimal locations for handling thin and flexible objects in Sec. IV-B1, we utilised an RGB-D camera to estimate the grasping poses in the real world. To simplify the detection of corners on various thin and flexible objects, we attach an ArUco marker to the corner as shown in Fig. 11-(a). With the known side length of the ArUco marker, we can estimate the transformation matrix from the camera's coordinate system to the marker's coordinate system, denoted as  $\mathbf{T}_C^M$ . This is achieved by minimising reprojection error through non-linear optimisation. To account for estimation errors that can occur with ArUco markers in real-world applications, we use depth information to adjust the estimated  $\mathbf{T}_C^M$ . First, we crop the depth map around the corners, similar to the approach in [1], to fit the object plane. Then, we adjust the rotation matrix of  $\mathbf{T}_C^M$  to be parallel to the depth-fitted plane, and we update the translation vector of  $\mathbf{T}_C^M$  based on the depth of the ArUco marker centre. Then, the target pose in the world frame represented with the transformation matrix  $\mathbf{T}_W^T$  can be calculated as:

$$\mathbf{T}_W^T = \mathbf{T}_W^E * \mathbf{T}_E^C * \mathbf{T}_C^M * \mathbf{T}_M^T, \quad (13)$$

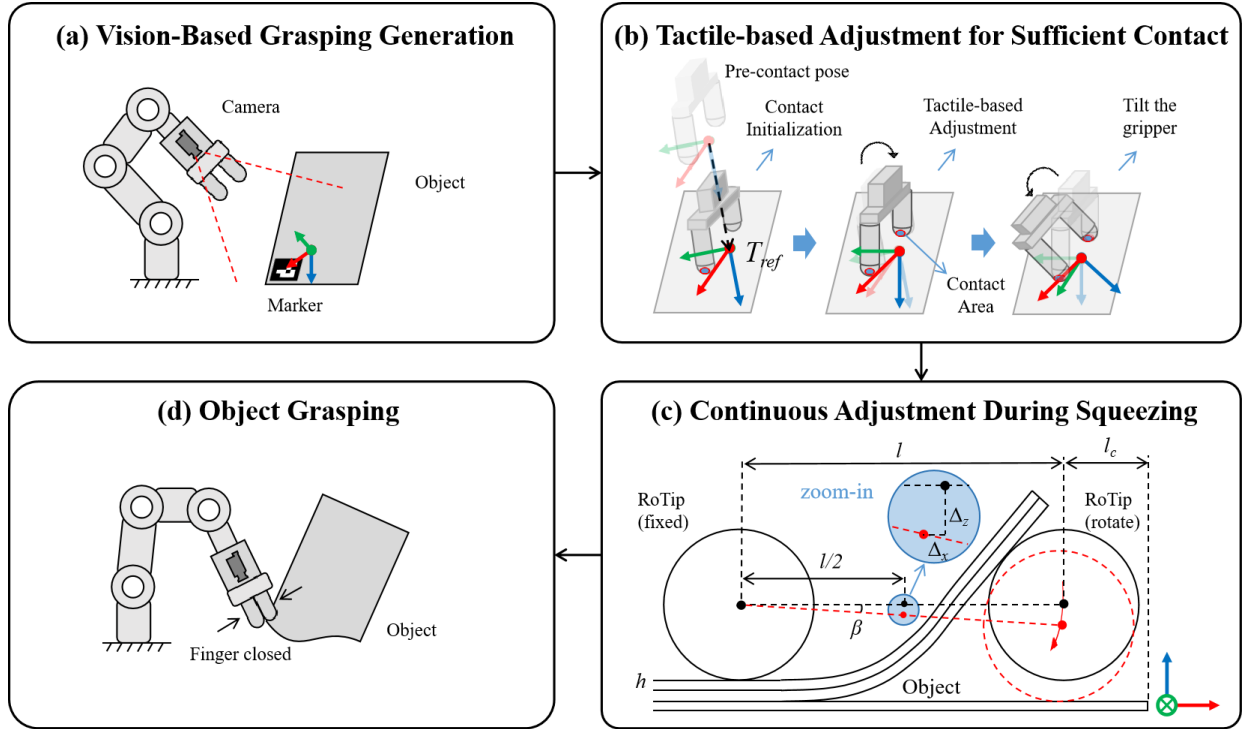


Fig. 11: An overview of our RoTipBot for thin and flexible handling. (a) **Vision-Based Grasping Generation**: Given an RGB-D image obtained from a camera, we generate the grasp proposal for guiding the robot to contact and grasp the object. (b) **Tactile-based Adjustment for Two-finger Sufficient Contact**: To compensate for the noise from visual perception, RoTip’s sensing capability is then utilised to adjust the robot’s end-effector. Once both RoTip sensors are in contact with the object, the end-effector will be rotated around its  $x$ -axis to an angle inclined to the object for feeding and grasping. (c) **Continuous Adjustment**: A continuous pose adjustment approach is proposed to ensure two-finger contact while feeding multiple thin and flexible objects. (d) **Object Grasping**: Finally, the gripper is closed to pick up the objects.

where  $\mathbf{T}_W^E$  represents the transformation matrix of the end-effector in the world coordinate;  $\mathbf{T}_E^C$  and  $\mathbf{T}_M^T$  represent the transformation matrix from the end-effector coordinate system to the camera coordinate system and from the marker coordinate system to the target coordinate system, respectively.

### C. Tactile-based Adjustment for Thin and Flexible Object Handling

Given an estimated target pose from Sec. IV-B2, moving directly to the target pose may result in collisions or insufficient contact due to the inherent positioning uncertainty of the vision system. Therefore, in this subsection, we introduce a tactile-based adjustment method that ensures both fingers securely contact thin, flexible objects to guarantee a secure grasp, i.e., two-finger contact. This method comprises three key steps, i.e., initial contact, pose adjustment and feeding for grasping, as shown in Fig. 11-(b) and (c). These steps are detailed as follows:

- **Contact Initialisation.** The end-effector is moved to a pre-contact pose, positioned with a translational offset along the  $z$ -axis relative to the target pose. A normal contact motion, using feedback control as described in Sec. IV-C1, guides the robot towards the object, and terminates when a RoTip finger makes initial contact with the object.
- **Pose Adjustment.** After establishing the initial contact, tactile-based adjustment refines the end-effector’s orientation to ensure that both RoTip sensors are in sufficient contact with the object. This step addresses the inherent

positioning uncertainty of the vision system. As detailed in Section IV-C2, if the contact area of the RoTip sensor exceeds an empirical threshold, it is recognised as a **sufficient contact**.

- **Feeding for Grasping.** Once both RoTip sensors establish contact with the object, the end-effector is rotated around its  $x$ -axis to incline towards the object, facilitating the feeding and grasping process. To handle multiple sheets of thin and flexible objects, we introduce a continuous adjustment approach, as described in Sec. IV-C3, to ensure both fingers maintain contact throughout the process, guaranteeing secure grasping.

1) *Feedback Control:* For the feedback control, we define the pose error  $\mathbf{E}_T$  as the  $SE(3)$  transformation that moves the observed pose  $\mathbf{T}_W^O$  to the target pose  $\mathbf{T}_W^T$  in the same coordinate frame:

$$\mathbf{E}_T = (\mathbf{T}_W^O)^{-1} \mathbf{T}_W^T. \quad (14)$$

To define the control operations, we project this pose error into the exponential coordinates for the Lie algebra  $\mathfrak{se}(3)$ , mapped onto the vector tangent space  $\mathbb{R}^6$ :

$$\mathbf{e}_T = \ln(\mathbf{E}_T)^\vee. \quad (15)$$

As shown in Alg. 1 (lines 6-10), there are two steps in establishing the contact: When the gripper is far from the object, the Euclidean normal of  $\mathbf{e}_T$ ’s translation component is larger than a predefined threshold  $\epsilon$  (set as 0.02 in our case), i.e.,  $\|\mathbf{e}_T[0 : 3]\| > \epsilon$ , a PD controller is used to control the robot to approach the surface of the thin and flexible object,

---

**Algorithm 1** Tactile-based Adjustment for Two-Finger Contact

---

```

1: Move to a pre-contact pose based on the target pose  $\mathbf{T}_{\text{ref}}$ 
2: Number of sufficient contact fingers:  $N = 0$ 
3: Pose Error:  $\mathbf{e}_{\mathbf{T}} = \ln(\mathbf{T}^{-1}\mathbf{T}_{\text{ref}})^{\vee}$ .
4: while True do
5:   if  $N == 0$  then   Sec. IV-C1 Contact Initialisation
6:     if  $\|\mathbf{e}_{\mathbf{T}}[0 : 3]\| > \epsilon$  then
7:        $\mathbf{u}(t) = \mathbf{K}_p \mathbf{e}_{\mathbf{T}}(t) + \mathbf{K}_d \frac{d\mathbf{e}_{\mathbf{T}}}{dt}(t)$ ,
8:     else
9:        $\mathbf{u}(t) = \mathbf{v}(t)$ 
10:    end if
11:   else if  $N == 1$  then   Sec. IV-C2 Pose Adjustment
12:      $\mathbf{T}_{\text{ref}} = \mathbf{T}_{\text{ref}} * [\mathbf{R}, \mathbf{0}]$ 
13:     Move to the refined pre-contact pose
14:      $N = 0$ 
15:   else if  $N == 2$  then
16:     Break
17:   end if
18:   update  $\mathbf{e}_{\mathbf{T}}$  and  $N$ 
19: end while

```

---

i.e.,  $\mathbf{u}(t) = \mathbf{K}_p \mathbf{e}_{\mathbf{T}}(t) + \mathbf{K}_d \frac{d\mathbf{e}_{\mathbf{T}}}{dt}(t)$ , where  $\mathbf{K}_p$  and  $\mathbf{K}_d$  are  $6 \times 6$  diagonal gain matrices associated with the error and derivative errors at time  $t$ . Once the gripper is close enough to the object, i.e.,  $\|\mathbf{e}_{\mathbf{T}}[0 : 3]\| \leq \epsilon$ , a feedforward control  $\mathbf{v}(t)$  is taken for  $\mathbf{u}(t)$  to move the end-effector towards the grasp pose to simplify the control.

2) *Pose Adjustment for Two-Finger Contact*: To ensure both RoTip sensors make sufficient contact with the object and achieve two-finger contact, the end-effector pose must be refined based on the tactile feedback. Specifically, achieving two-finger contact involves aligning the end-effector  $z$ -axis normal vector  $\mathbf{n}_1$  with the contact plane normal vector  $\mathbf{n}_2$  estimated in Sec. III-C3. This alignment can be achieved by calculating the rotation matrix  $\mathbf{R}$  to adjust the end-effector pose using Rodrigues' formula as follows:

$$\mathbf{R} = \mathbf{I} + (\sin \theta)\mathbf{A} + (1 - \cos \theta)\mathbf{A}^2 \quad (16)$$

where  $\theta = \arccos(\mathbf{n}_1 \cdot \mathbf{n}_2)$  is the rotation angle and  $\mathbf{A}$  is the skew-symmetric matrix of the rotation axis  $\mathbf{a} = [a_x, a_y, a_z] = \mathbf{n}_1 \times \mathbf{n}_2$ :

$$\mathbf{A} = \begin{pmatrix} 0 & -a_z & a_y \\ a_z & 0 & -a_x \\ -a_y & a_x & 0 \end{pmatrix}. \quad (17)$$

3) *Continuous Adjustment for Efficient Feeding*: Although the initial pose adjustment in Sec. IV-C2 could secure two-finger contact at the beginning, continuous adjustment of the end-effector is necessary to address the changes in the stacked thickness during the feeding of multiple sheets, as shown in Fig. 11-(c). This requires a 3-dimensional adjustment ( $\beta, \Delta_x, \Delta_z$ ) to refine the end-effector pose:

$$\begin{cases} \beta & = \arcsin \frac{n \cdot h}{l} \\ \Delta_x & = -l/2 * (1 - \cos \beta) \\ \Delta_z & = -l/2 * \sin \beta \end{cases} \quad (18)$$

where  $\beta$  is the rotational adjustment along the  $y$ -axis, and  $\Delta_x$  and  $\Delta_z$  are the translational adjustments along the  $x$ -axis and  $z$ -axis of the local coordinate, respectively. The axes of the local coordinate are represented with Red, Green and Blue arrows at the right corner of Fig. 11-(c). Here,  $n$ ,  $h$  and  $l$  represent the number of fed layers, the thickness of each layer, and the distance between two RoTip sensors, respectively. This adjustment must then be transformed from the current local coordinate system to the world coordinate system.

## V. EXPERIMENTAL RESULTS

In this section, we will conduct comprehensive experiments to evaluate our proposed RoTipBot approach for handling thin and flexible objects. The experiments will focus on four key aspects: (1) identifying the optimal grasping locations for handling these objects; (2) exploring the significance of tactile-based adjustment to ensure consistent two-finger contact; (3) assessing the effectiveness of the continuous adjustment with different kinds of thin and flexible objects against the state-of-the-art approaches; and (4) exploring additional applications with our RoTip sensors.

### A. Experiments on Grasp Position Analysis

In this subsection, we conduct two experiments to verify the theoretical analysis in Sec. IV-B1, which concludes that the corners of thin and flexible objects are the optimal locations for squeezing and feeding. Specifically, we perform experiments to compare the force applied to the object during squeezing, and to determine the total number of thin and flexible objects (using papers as an example) grasped at various locations with different applied normal forces.

1) *Comparison of Required Forces*: To compare the forces during the squeezing of thin and flexible objects, we employ both Finite Element Method (FEM) in simulation and a force sensor in real-world experiments, as shown in Fig. 12.

In the simulation test, FEM is used to simulate the interaction between the RoTip fingers and the object at different locations. The process involves two steps: first, two fingers press the object; then, one of the fingers squeezes the paper by sliding. The simulation provides precise force estimations exerted by the object and visualises the displacement distribution. Details of the simulation configuration are provided in Appendix A.

To verify the FEA results, we conducted a real-world experiment. A Nano 17 force/torque sensor was employed to measure the forces exerted while squeezing the object. This sensor was attached to the end-effector of the UR5e robotic arm, as shown in Fig. 12 (right column), where a blue quadrangular area was secured to the table using double-sided tape to simulate the pressing of the passive finger. Although the RoTip sensor has the potential to measure applied force, it does not match the precision of the Nano 17, which is commonly used in previous research [9], [18], [39] as a benchmark for ground truth.

We performed the squeezing action at various locations on the object, i.e., the centre, edge, and corners. Squeezing the object at its corner is divided into two distinct scenarios,

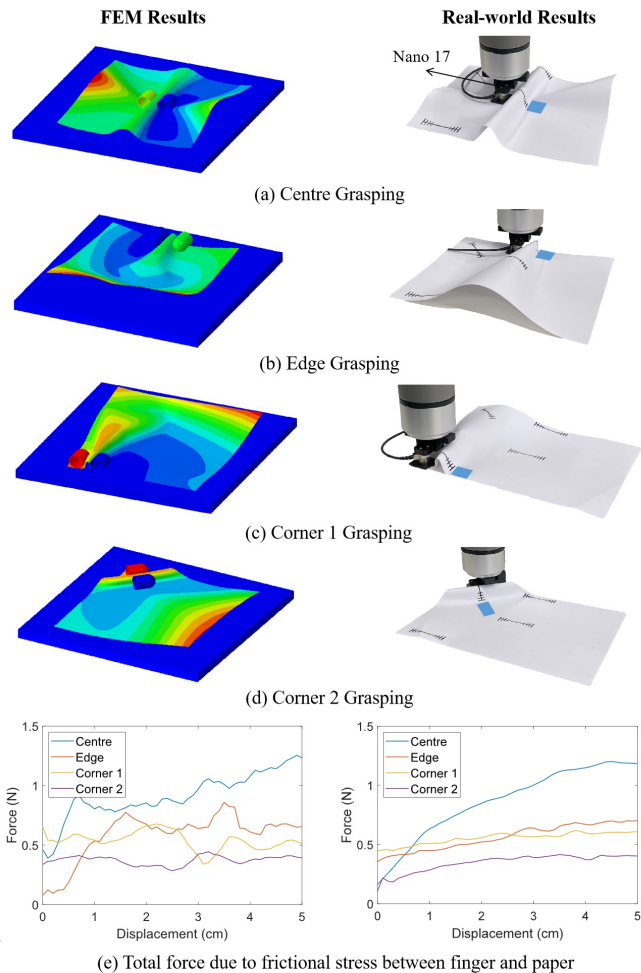


Fig. 12: Comparison of required forces when squeezing different locations. The left and right columns show the FEM results and real-world results for estimating the elastic force of the object, respectively. The first four rows show experiments at different locations (i.e., centre, edge, and corners). The last row presents the force plots for squeezing the paper. The results indicate that squeezing along the angle bisector of the object’s corner (d) results in the smallest elastic force, thereby requiring the least squeezing force.

each defined by the direction of applied force. In Case 1, the squeezing is executed parallel to the object’s edge, as shown in Fig. 12-(c). Case 2 involves squeezing along the angle bisector of the object corner, as depicted in Fig. 12-(d).

As shown on the left of Fig. 12-(e), the maximum forces applied by the object show a clear pattern: the centre is the hardest to squeeze, followed by the edges, and finally the corners. Furthermore, squeezing along the angle bisector of the object corner results in the smallest maximum force. In our real-world experiments, the same trend is observed, with the corner cases involving smaller squeezing forces. Specifically, the average maximum force applied by the object at the corner (Case 2) was measured at 0.419N, which is notably lower than the forces measured at the corner (Case 1) (0.731N), edge (0.753N) and centre (1.246N). These findings validate the conclusions drawn from our theoretical analysis in Sec. IV-B1. Moreover, both the FEM visualisation of displacement distribution and real-world snapshots indicate that when squeezing at the corners, the object moves less vigorously around the fingertip, reducing the likelihood of damaging the object.

TABLE II: The number of pages squeezed and grasped at different locations.

Normal Force	Centre	Edge	Corner 1	Corner 2
2N	0	0	2	4
4N	0	1	13	13
6N	0	4	18	20
8N	1	5	23	23
10N	4	5	25	25
2-10N	5	15	81	85

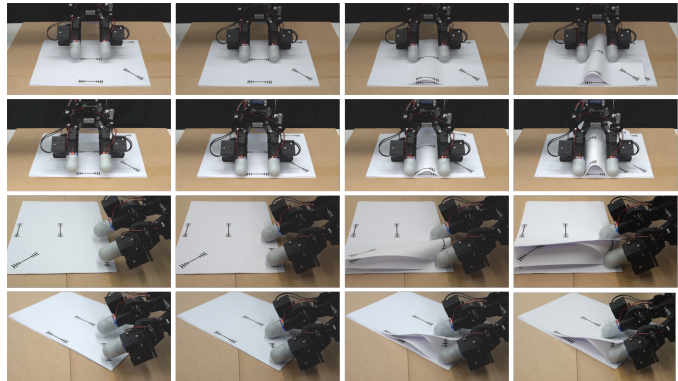


Fig. 13: Snapshots of squeezing at different locations. From top to bottom: the centre, the edge, and the corner (two cases). During the 5-second squeezing, only one page can be squeezed at the centre and edge, while multiple pages can be squeezed at the corners. When squeezing along the angle bisector of the object corner (Case 2), the deformation of the printer paper is less intense.

2) *Grasping Performance at Different Locations:* To verify that grasping at the corners is the most effective, we conducted grasping experiments in a real-world setting. Our evaluation of performance relied on the key metric of the total number of grasped papers. For simplicity, the grasp positions were predetermined in this experiment, eliminating the need for tactile-based adjustments. This setup ensured that both fingers were in firm contact with the object during each grasp attempt.

In this experiment, we altered the normal force between the RoTip and the object, ranging from 2N to 10N in increments of 2N. In such a way, the increment of each finger is 1N. Additionally, we maintained a constant actuator speed, set at 90 degrees per second for 5 seconds. After that, the gripper is closed to pick up the object. The numbers in Table II represent the total number of pages squeezed in 5 trials for each force. Table II shows that squeezing objects around corners leads to the largest number of grasped papers. Furthermore, we captured snapshots of the squeezing process at different locations, shown in Fig. 13. When squeezing along the angle bisector of the object corner (Case 2), the deformation of the printer paper is less intense.

### B. Tactile-based Adjustment for Two-finger Contact

In this subsection, we conduct a series of experiments to evaluate the tactile-based adjustment in achieving two-finger contact, a crucial requirement for manipulating the objects. We focus on two key aspects: the accuracy of plane fitting using different modalities, i.e., vision, force sensing and tactile feedback; and the overall success rate of contact between RoTip sensors and the thin and flexible object.

1) *Experiments on Plane Estimation:* We evaluate the accuracy of three different sensing modalities: a vision-based

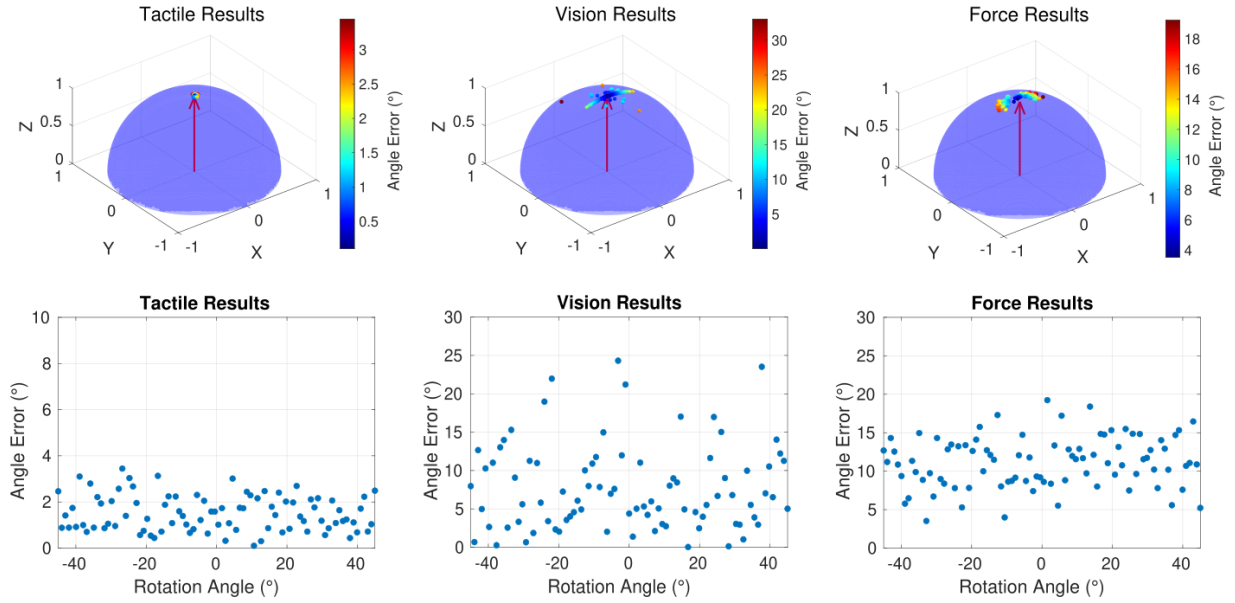


Fig. 14: Experiments on contact plane estimation. **Top Row:** The visualisation of the normal vector of the estimated plane. **Bottom Row:** Quantitative plots show that contact planes estimated through tactile perception exhibit superior accuracy compared to those derived from visual and force information.

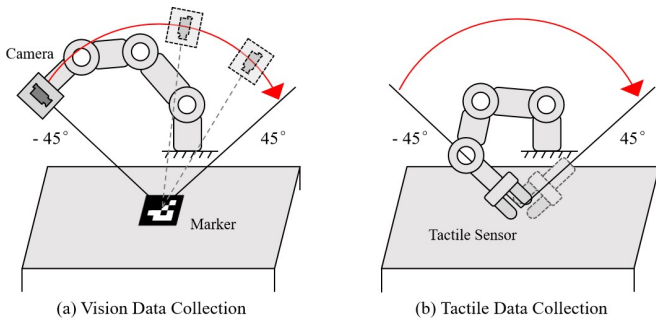


Fig. 15: Sketch for (a) visual data collection and (b) tactile and force data collection. The rotation spans from  $-45^\circ$  to  $45^\circ$ , with each increment of  $1^\circ$ .

system using ArUco markers in Sec. IV-B2, force sensing integrated into the UR5e robotic arm, and our proposed tactile contact plane estimation in Sec. V-B1. To facilitate this comparison, we collect the data from those different sensing modalities as shown in Fig. 15.

We adjust the rotation angle of the end-effector equipped with RoTip sensors, followed by remote observation of the ArUco Marker on the table and physical contact with it. The rotation spans from  $-45^\circ$  to  $45^\circ$ , with each increment of  $1^\circ$ . The ground truth for the normal contact plane remains parallel to the  $z$ -axis of the world frame, as the marker is taped to the table upon which the robotic arm's base is situated. Hence, the ground truth is represented by the vector  $(0, 0, 1)$ , as shown in the first row of Fig. 14. The accuracy is evaluated through the angle error  $e_n$  between the ground truth normal vector  $\mathbf{n}_{\text{real}}$  and the estimated normal vector  $\mathbf{n}_{\text{estimated}}$  of the plane, computed as follows:

$$e_n = \arccos(\mathbf{n}_{\text{estimated}} \cdot \mathbf{n}_{\text{real}}). \quad (19)$$

Similar to the coordinate transformation in Eq. 13, the ArUco marker coordinate estimated with vision can be calculated through  $\mathbf{R}_W^M = \mathbf{R}_W^E * \mathbf{R}_E^C * \mathbf{R}_C^M$ , where  $\mathbf{R}_A^B$  represents

the rotation matrix from  $A$  coordinate to  $B$  coordinate. The third column of  $\mathbf{R}_W^M$  represents the plane surface normal vector in the world frame. To estimate the plane normal with the UR5e integrated force sensor, we first obtain the wrench data from the UR5e's ROS (Robot Operating System) driver. Then, we transform the wrench data referenced in the end-effector coordinate to the world coordinate.

In the top row of Fig. 14, each point represents a normalised surface vector estimated with corresponding sensing modalities. A more concentrated distribution of these points indicates a higher accuracy in the estimation results. Notably, our RoTip sensor demonstrates significantly higher accuracy in sensing the plane surface compared to both the force sensing and the vision system. We analysed the angle error using Eq. 19, revealing that our approach achieves accurate plane estimation with an average error of  $1.51^\circ$ . It significantly outperforms vision system-based and integrated force sensing methods, which have an average error of  $7.82^\circ$  and  $11.14^\circ$ , respectively. Additionally, the visualisation of angle errors in the bottom row of Fig. 14 confirms the superior accuracy of our tactile plane estimation approach.

Similar to the approach described in [1], we restrict our use of depth information to the area surrounding the corners of the object. Hence, the primary sources of error in the vision system are attributed to noise within the depth-fitted plane and insufficient depth information. Although utilising the depth information from the entire table could significantly enhance performance, we refrain from doing so due to the challenge of ensuring that the table remains perfectly flat at all times. On the other hand, the discrepancy of the force sensing likely arises from the accuracy of the integrated F/T sensor and the elastomer's deformation, which may generate applied force in the horizontal direction. While the utilisation of an advanced force sensor could potentially reduce estimation errors, it would come at a higher cost. As a result, our RoTip sensors

TABLE III: The success rates of two-finger contact experiments.

Approach	One-Finger SR	Two-Finger SR
Vision	0.50	0.30
Vision + Force (WA)	1.0	0.50
Vision + Force	1.0	0.55
Vision + Force + Tactile (Ours)	1.0	1.0

WA: Without Adjustment.

provide an affordable solution for sensing thin and flexible objects while maintaining accurate sensing performance.

2) *Experiments on Two-finger Contact*: Subsequently, we evaluate the success rate of achieving contact after adjusting the end-effector pose using various plane fitting approaches. A successful contact is defined by the contact areas detected by the RoTip sensor exceeding a predefined threshold. Since the Robotiq gripper is equipped with two RoTip sensors, our evaluation includes both the success rate of single-finger contact and two-finger contact.

We tested four different plane estimation approaches with 20 trials each to evaluate the contact success rate, as shown in Table III. The “Vision” method directly guides the end-effector to the target position. The “Vision + Force (WA)” method positions the end-effector to a pre-contact pose and establishes normal contact, halting movement when the force exceeds a certain threshold. The “Vision + Force” method refines the target pose by integrating plane estimation from force sensing. Our proposed “Vision + Force +Tactile” method adjusts the target pose based on the results of tactile plane estimation and uses force measurements to control the robot.

As reported in Table III, achieving two-finger contact relying solely on vision is challenging. Even one-finger contact cannot be ensured due to translation errors in grasp pose estimation. At times, the end-effector is positioned slightly away from the object, while at other times, it is too close, triggering an emergency stop. The “Vision + Force (WA)” and “Vision + Force” methods improve the reliability of one-finger contact but lack the precision needed for two-finger contact. Although the vision-based method has a lower average plane fitting error, the plane normal error in the  $y$ -axis significantly affects the height difference between the fingertips of two RoTip sensors, impacting the success rate of contact. As shown in the top row of Fig. 14, the  $y$ -axis error for plane estimation using force data is similar to that of vision, resulting in comparable contact success rates. Our proposed method, which integrates vision, force sensing and tactile sensing, not only ensures one-finger contact but also significantly enhances the accuracy of achieving two-finger contact, with a success rate of 100%. This two-finger contact is crucial for handling thin and flexible objects: If the passive finger used to hold the object loses contact, the object will slide on the table during the rotation of the active finger. In contrast, if the active finger used for rotation loses contact, the object cannot be manipulated.

### C. Experiments on thin and flexible object handling

In this subsection, we conduct comprehensive experiments to evaluate our proposed RoTipBot approach for handling

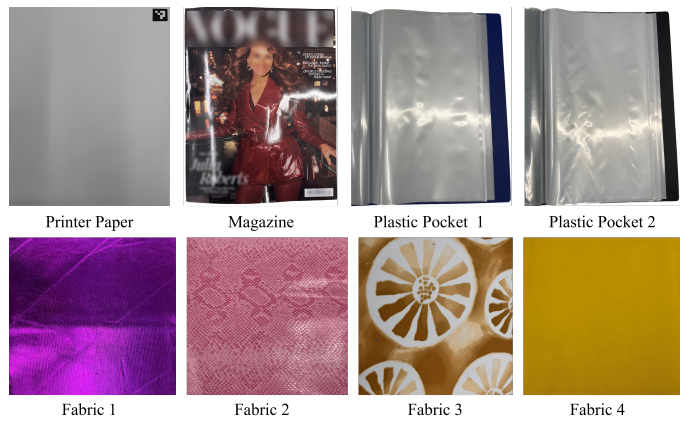


Fig. 16: Objects used in our experiments. **From left to right**: Top row includes printer paper, coated paper (magazine) and two plastic pocket sheets for comparing against the SOTA methods [1], [8]. The bottom row includes four fabrics with different stiffness and textures, used to test the generalisation ability of our proposed approach.

TABLE IV: The time taken to feed each page.

Page index	1-3	4-6	7-9	10-12
wo/CA	$1.14 \pm 0.30$	$1.78 \pm 0.80$	N/A	N/A
w/CA	$0.98 \pm 0.15$	$0.83 \pm 0.13$	$0.93 \pm 0.12$	$0.84 \pm 0.13$

CA: Continuous Adjustment.

thin and flexible objects. First, we evaluate the importance of the continuous adjustment proposed in Sec. IV-C3. Then, we compare our proposed method against the state-of-the-art (SOTA) methods [1], [8]. Finally, we test the generalisation ability of our method and showcase the failure cases during thin and flexible object handling.

The objects used in this study are shown in Fig. 16. Among these, printer paper, coated paper and plastic sheets are used for the comparison against the SOTA methods, while four different fabrics are used in the test of generalisation ability of our method. Printer paper exhibits the highest elasticity, coated paper (magazine) has the lowest elasticity, and plastic pocket sheets fall in between with medium elasticity.

1) *Experiments on Continuous Adjustment*: We first assess the importance of continuous adjustment. Specifically, we placed 15 sheets of printer paper on the table for feeding and grasping, and set the initial applied normal force of each finger to 4N. To minimise uncertainty in the visual system, objects were placed in predefined locations. The evaluation metric used here is the time required to feed each sheet.

We recorded the time required to feed each sheet with and without continuous adjustments. As shown in Table IV, for the first three sheets, when contact is sufficient, continuous adjustments have minimal effect. However, as more sheets are fed, contact becomes increasingly inadequate. Without continuous adjustment, the time to feed each sheet increases significantly, and only the first six sheets could be consistently fed. The robot fails to feed beyond six sheets (marked as N/A in Table IV for the 7-9 and 10-12 cases). In contrast, all sheets can be successfully fed when continuous adjustment is used. We also visualise the feeding time for each sheet with a box plot in Fig. 17. This plot shows that our proposed RoTipBot with continuous adjustment maintains a consistent average feeding time and a small variance across all sheets, unlike the

TABLE V: Comparison of grasping Success Rate (SR) and the operation speed, i.e., Pages Per Minute (PPM).

Approach	Angle	Multi-page Grasping	Printer paper		Coated paper		Plastic pocket sheet		All	
			SR ↑	PPM ↑	SR ↑	PPM ↑	SR ↑	PPM ↑	SR ↑	PPM ↑
Flex&Flip [8]	60°	×	60%	3.10	57%	2.95	43%	2.59	53.3%	2.88
FlipBot [1]		×	83%	4.28	81%	4.18	68%	3.52	77.3%	3.99
RoTipBot (Ours)		✓	<b>90%</b>	<b>12.3</b>	<b>87%</b>	<b>10.9</b>	<b>94%</b>	<b>11.3</b>	<b>90.3%</b>	<b>11.5</b>
Flex&Flip [8]	30°	×	69%	3.57	73%	3.77	43%	2.22	61.7%	3.19
FlipBot [1]		×	91%	4.68	91%	4.70	67%	3.46	83.0%	4.28
RoTipBot (Ours)		✓	<b>92%</b>	<b>11.7</b>	<b>89%</b>	<b>11.2</b>	<b>93%</b>	<b>11.5</b>	<b>91.3%</b>	<b>11.5</b>
Flex&Flip [8]	0°	×	71%	3.65	80%	4.11	51%	2.61	67.3%	3.46
FlipBot [1]		×	92%	4.75	95%	4.91	75%	3.88	87.3%	4.51
RoTipBot (Ours)		✓	<b>92%</b>	<b>12.1</b>	<b>90%</b>	<b>11.5</b>	<b>94%</b>	<b>11.8</b>	<b>92.0%</b>	<b>11.8</b>

Note: The results for FlipBot [1] and Flex&Flip [8] are copied from the SOTA FlipBot paper [1].

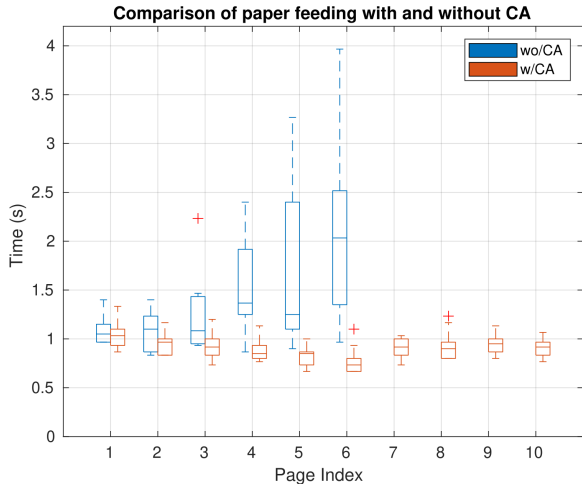


Fig. 17: Box plot of the feeding time taken for each sheet, with and without continuous adjustment. Our proposed continuous adjustment maintains a consistently low feeding time for all sheets with minimal variance. In contrast, without continuous adjustment, the feeding time per sheet gradually increases with higher variance, and the system fails to feed beyond six sheets (hence, no plots for wo/CA beyond six sheets in the figure).

increasing feeding time and higher variance observed without continuous adjustment. This consistency is crucial for tasks that require precise processing and handling of multiple thin and flexible objects.

2) *Comparison against SOTA*: Following the benchmarks set by the SOTA FlipBot approach [1], we evaluate our proposed approach using both Success Rate (SR) and Pages Per Minute (PPM) metrics, providing a comprehensive assessment of its effectiveness and efficiency. Unlike FlipBot [1], which is limited to grasping a single sheet at a time, our RoTipBot can grasp multiple sheets in one trial. Hence, we conduct ten repetitions for each trial with a target set at ten pages and define the SR as follows:

$$SR = 1 - \frac{|\text{Grasped Number} - \text{Target Number}|}{\text{Target Number}} \quad (20)$$

In this experiment, three types of thin and flexible objects with different physical properties were used, i.e., printer paper, coated paper, and plastic pocket sheet, consistent with those used in [1]. This selection allowed for a direct comparison of our RoTipBot against SOTA methods. To test the effect of gravity on paper flipping, we placed the object on a laptop stand, as shown in Fig. 8, and varied its tilt angles at 0, 30, and 60 degrees.

As shown in Table V, our RoTipBot consistently achieves more than a 90% success rate regardless of the tilt angle. Moreover, RoTipBot outperforms the SOTA method [1] in terms of overall success rate across various angles, achieving up to a 13% improvement at 60° and at least a 5% improvement at 0°. More importantly, RoTipBot operates significantly faster than the SOTA approaches, achieving speeds up to three times faster. We also show snapshots of grasping different objects at various tilt angles in Fig. 18 for visualisation.

Specifically for different objects, our method modestly outperforms the SOTA with printed papers and significantly enhances success rates for plastic pocket sheets, showing a minimum improvement of 19%, across different angles. However, coated papers present the most significant challenge, with slightly lower performance compared to the SOTA when grasping at 0° and 30°. This performance gap deviates from the results of FlipBot [1], where our method excels at grasping plastic pocket sheets compared to coated paper, contrary to the trends observed in FlipBot. The challenge with coated papers stems from their softness and lack of elasticity, making them more susceptible to gravity. This either causes creasing that hinders the handling, or makes it difficult to feed them completely between the two RoTip sensors. In contrast, printer papers and plastic pocket sheets have stronger elasticity, which helps avoid creasing issues. However, ArUco markers printed on printer papers can introduce static electricity, complicating separation and reducing grasping performance compared to plastic sheets. Moreover, tiny protrusions on the edges of plastic sheets create small gaps between layers, preventing van der Waals forces from hindering movement [49]. This makes separation easier and facilitates more efficient grasping.

Our RoTipBot currently operates at a speed significantly below its maximum capability. The actuator in RoTip sensors rotates at 90 degrees per second, though it can achieve speeds up to 276 degrees per second. Theoretically, the feeding speed could be tripled by increasing the actuator speed. However, higher speeds compromise accuracy due to dynamic errors. It is also important to note that the majority of the operation time is consumed by initial contact and subsequent tactile-based adjustments, taking 30 to 35 seconds, while feeding and grasping objects require only about 10 seconds. Implementing impedance control, which adjusts the end-effector’s pose while maintaining contact, could reduce the time required for these adjustments.

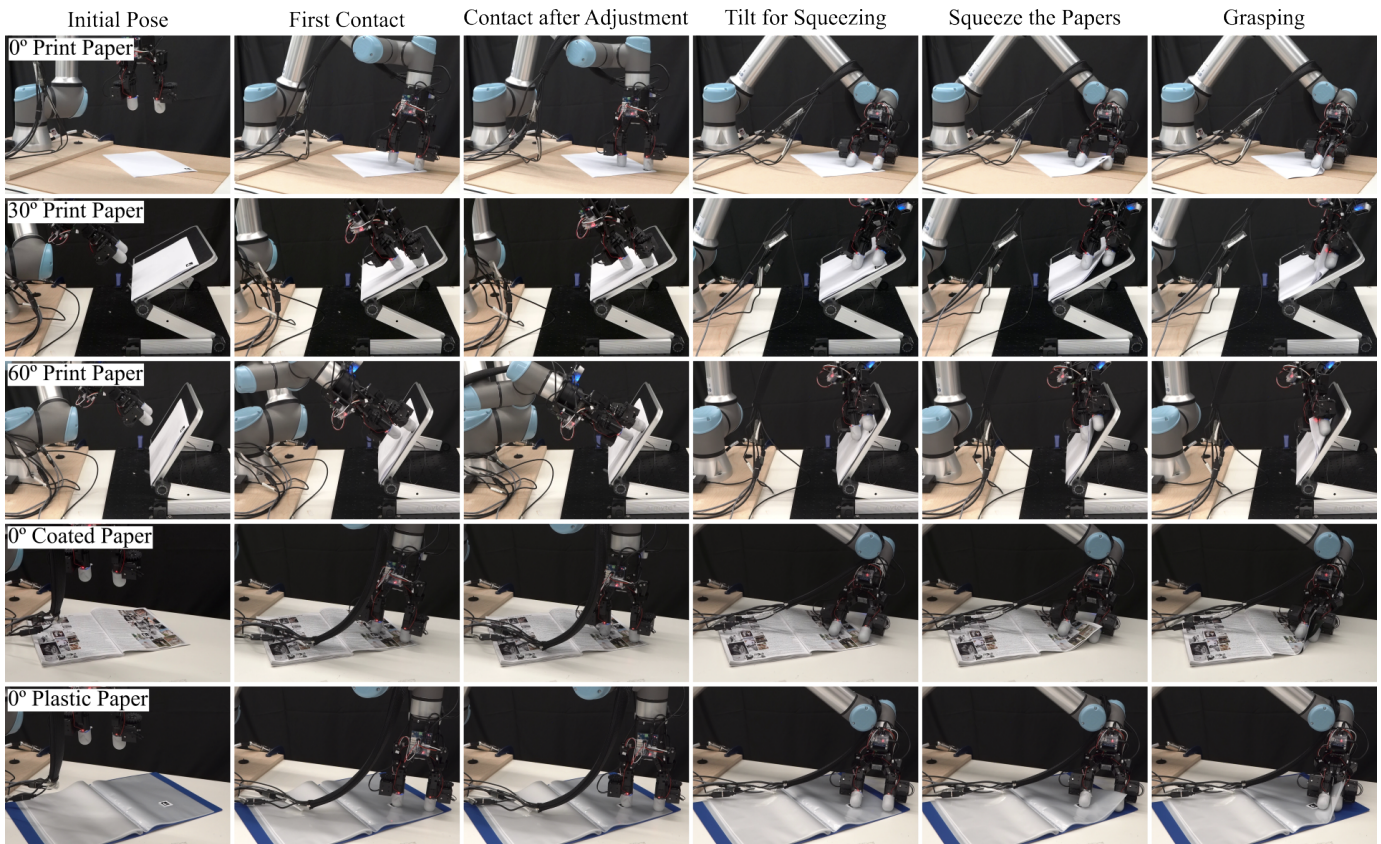


Fig. 18: Snapshots of the contact and grasping stages. The first three rows show the grasping of printer papers at 0°, 30° and 60°. The last two rows show the grasping of coated papers and plastic pocket sheets. For each row, from the left to right: initial pose, first one-finger contact, two-finger contact after tactile-based adjustment, tilting to feed the paper, feeding the papers, and closing the gripper to grasp.



Fig. 19: Snapshots of grasping four different fabrics. **First column:** The Robotiq gripper equipped with RoTip sensors first moves down to touch the fabric. **Second and third columns:** Then, one RoTip sensor squeezes the fabric to feed it between the two RoTip sensors. **Last column:** Finally, the gripper is closed to hold the fabric.

3) *Generalisation and Other Applications:* The generalisation of our RoTipBot was further evaluated through tests on four distinct types of fabrics as shown in the bottom row of Fig. 16. RoTipBot achieved a nearly perfect success rate in grasping across various fabric types, approaching 100%, as demonstrated in Fig. 19.

Furthermore, we extended the application of our RoTipBot to the manipulation of a hex key and an oyster card, as illustrated in Fig. 20. By rotating the RoTip fingers in the same direction, the hex key is spun along its vertical axis.

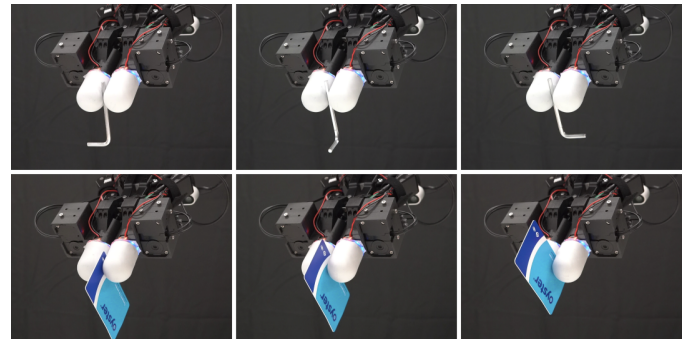


Fig. 20: Snapshots showcasing other applications of RoTipBot. **Top Row:** When both RoTip fingers rotate clockwise, the hex key spins along its vertical axis. **Bottom Row:** When the RoTip fingers rotate in opposite directions, they manipulate the oyster card through translational movement.

In contrast, the bottom row of Fig. 20 demonstrates how the RoTip fingers, rotating in opposing directions, induce translational movement in the oyster card.

These experiments underscore the precision and versatility of our RoTipBot in handling objects of diverse shapes and sizes. From delicately manipulating thin fabrics to executing intricate manoeuvres with the hex key and oyster card, our RoTipBot demonstrates remarkable proficiency and potential for a wide range of practical applications. The success of RoTipBot paves the way for future research into using rotatable tactile sensors for various object manipulation tasks.

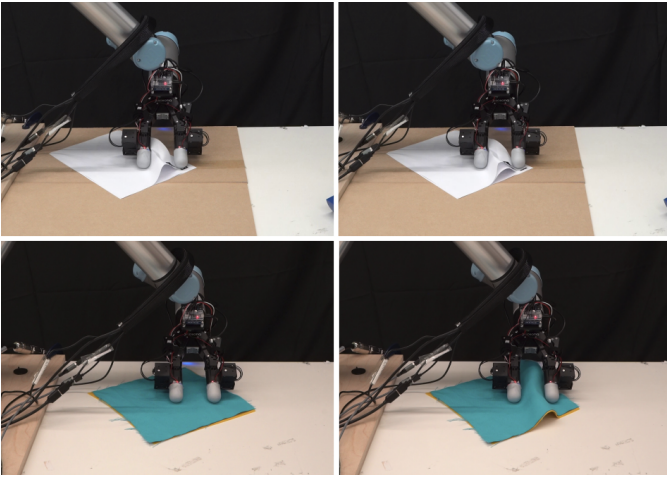


Fig. 21: **Visualisation of Failure Cases.** The first row shows that the printer paper with wrinkles is hard to squeeze and stops the next page’s movement, eventually leading to a feeding failure. The second row demonstrates a failure case when grasping objects with a high friction coefficient, where two layers of fabrics are squeezed together.

4) *Failure Cases:* While our experiments demonstrated the effectiveness of our RoTipBot across a spectrum of applications, our real-world trials also brought to light some failure cases, as outlined below:

- **Incorrect object counts during grasping:** The issue arises due to the imprecise positioning of RoTip sensors, either too close or too far from corners, when the vision system is unable to identify and target the grasp locations accurately. This leads to a disparity in the feeding speed: grasp positions nearer to the corner result in a faster-than-expected feeding motion and result in grasping more pages than expected. Conversely, when the grasp position is farther from a corner, the feeding action tends to be slower, which results in fewer pages being grasped. To address this issue, the actuator speed could be adjusted in real time for precise handling.
- **Inadequate force applied to objects with wrinkles:** When handling stiff objects with wrinkles, such as crumpled printer papers and coated papers, the force distribution changes, leading to inadequate force being applied during manipulation. This issue is similar to a cash counting machine failing to process wrinkled currency. As shown in Fig. 21 (top row), wrinkled printer paper is difficult to squeeze, impeding the movement of the subsequent pages and causing handling failures. Integrating the RoTip sensors into a dexterous hand with a third finger could resolve this by applying additional force to manage the stuck paper.
- **Grasping objects with a high friction coefficient:** When the friction coefficient between the RoTip sensor and the object’s top surface is lower than that between the object’s layers, the finger’s squeezing action may not generate sufficient force to separate the top layer from the remaining layers. Furthermore, if the friction coefficient between the object and the table is lower than that between the finger and the object, multiple layers of the object may be squeezed and bent together, causing them to remain stuck to each other. This issue is particularly evident

TABLE VI: Comparison of passive and active rotatable tactile sensors.

	Passive Rotatable	Active Rotatable
<b>Pros</b>	Cost-effective, simple to implement	Precise control, applicable in a wide range of applications
<b>Cons</b>	Requires additional devices for full functionality	High complexity, increased costs
<b>Examples</b>	TouchRoller [20], Roller Tactile Sensor [51]	TacRot [21], TRRG [22], GelFinger [50], RoTip (ours)

when handling rough fabrics consisting of multiple layers, as illustrated in the bottom row of Fig. 21. A potential solution is to increase the friction coefficient of the tactile fingers by adding a textured surface. This adjustment would allow a light force to manipulate the top layer without affecting the other layers.

## VI. DISCUSSION

### A. Discussion on Rotatable Tactile Sensors

In recent years, advancements in vision-based tactile sensing have primarily centred on enhancing sensing precision and expanding the range of sensing modalities. There has been a movement towards making tactile sensors more dynamic or mobilised to meet the requirements for more skilful manipulation. This includes dynamically adjusting the camera’s position [50] or moving the sensor’s surface via rotation and translation motions [20], [51]. Specifically, tactile sensors that can rotate utilise two distinct strategies: passive rotation and active rotation, as summarised in Table VI.

Passive rotatable tactile sensors [20], [51] rely on the sensor’s ability to adjust its orientation in response to external forces without an active mechanism. This method is characterised by simplicity, low cost, and high efficiency, and is particularly suitable for environments where these attributes are prioritised, such as exploration and monitoring in harsh environments.

Active rotatable tactile sensors [21], [22], [50] involve the sensor itself moving, usually driven by an external actuator or motor. This allows for precise control of contact status and delicate manipulation of objects. This active movement is particularly advantageous in robotic applications requiring detailed interaction, such as assembly lines or household care. However, it introduces challenges like increased complexity, higher costs, and greater power consumption.

Compared to the previous active rotatable tactile sensors such as TacRot [21] and TRRG [22] that can only sense the inner side of the fingertip, our RoTip sensor is the first to provide tactile sensing across the entire fingertip area while enabling finger rotation. This mobilised omnidirectional tactile sensing significantly enhances dexterity. Consequently, RoTipBot is the first system to facilitate the grasping of thin and flexible objects with mobilised vision-based tactile sensing.

### B. Handling Policy for Thin and Flexible Objects

We employed the FEM due to its accuracy and reliability to determine the best locations for handling thin and flexible

objects. FEM excels in modelling and simulating the physical response of materials to various forces. Nonetheless, it also has certain limitations. However, it has certain limitations, particularly the significant computational resources required, especially when dealing with complex materials such as thin and flexible objects.

Conversely, Reinforcement Learning (RL) has gained attention as an effective method for interacting with objects and learning optimal behaviours through trial and error [1]. Unlike FEA, RL does not need exhaustive pre-defined material properties and can improve its accuracy with increased exposure to diverse situations. This adaptability allows RL to adjust to new objects and scenarios over time. However, RL usually starts with lower accuracy and requires significant data and computational investment during the learning phase.

In the future, it would be interesting to develop a hybrid approach that combines the accuracy of FEM with the adaptability and learning capabilities of RL. Such an integration could leverage FEM for initial detailed simulations, providing a foundational understanding that can be further refined and adapted through RL's interaction-based learning. This hybrid model could address the limitations of both methods, leading to more robust and efficient systems for handling thin and flexible objects.

### C. Discussion on Tactile-based Adjustment

Tactile-based adjustment, which involves adjusting the position and orientation of an object or a robot end-effector based on tactile feedback, has recently been used in various robotic applications [52]–[54]. For example, Hogan et al. [55] designed a tactile-based policy for grasp adjustment, which adjusts the end-effector pose and improves the grasping quality. Jiang et al. [56] leveraged tactile feedback from a vision-predicted poking point predicted to refine the grasping pose of transparent objects. Lloyd and Lepora [57], [58] used tactile feedback to adjust the end-effector's pose while exploring the object's surface.

Many of these studies employ vision-based tactile sensors, recognised as cost-effective alternatives to expensive force sensors. For instance, the GelSight Mini<sup>6</sup> and DIGIT [14] are priced around \$400, significantly lower than the ATI Nano17 and Robotiq force torque sensors, which can exceed \$5,000. Similarly, our proposed RoTip sensor is budget-friendly \$400, and provides accurate contact surface estimation, as shown in Fig. 14. By replacing the current actuator with a lite version, the cost can be reduced to less than \$200. As a result, the tactile-based adjustment proposed in this work with the RoTip sensor is both cost-effective and powerful for handling thin, flexible objects.

However, this does not imply that tactile-based adjustment is superior to force-based adjustment approaches in all aspects. Vision-based tactile sensors can experience delays due to the time needed to process extensive visual data. Although recent innovations have introduced event-based tactile sensors [59] with higher processing speeds, these sensors are considerably more expensive due to the costs associated with integrating

delicate event-based cameras. Consequently, force sensors and force-based adjustment approaches may offer better performance for tasks that demand high-frequency responses.

## VII. CONCLUSION

In this paper, we propose RoTipBot, a novel approach for handling thin and flexible objects using rotatable tactile sensors. We first develop RoTip, a tactile sensor capable of providing comprehensive contact information around the fingertip and actively rotating its body. RoTipBot leverages RoTip's rotation capability to feed multiple sheets into the centre between the two fingers, allowing them to be grasped simultaneously. Additionally, RoTip's sensing capability is used to ensure both fingers maintain firm contact with the object, which is crucial for the feeding motion. The results show that our RoTip sensor achieves plane estimation with a low average error of  $1.51^\circ$ . Moreover, our RoTipBot outperforms state-of-the-art methods in overall success rate and operates up to three times faster. The success of RoTipBot opens new research directions for other object manipulation tasks using mobilised tactile sensors.

In the future, we aim to miniaturise the RoTip sensor and integrate it into a dexterous hand to enhance its functionality and application potential. This advancement would enable more precise and versatile manipulation of a wide range of objects. Additionally, we plan to explore the use of reinforcement learning approaches to develop a general handling policy for different kinds of deformable objects, initially guided by Finite Element Analysis (FEA). This will equip the system with the ability to autonomously learn and adapt its manipulation strategies across a variety of scenarios. To further improve the applicability and accuracy of our approach in real-world situations, we will explore more general vision algorithms. For example, a deep learning-based corner detection model can be integrated to replace the current ArUco markers.

## APPENDIX A CONFIGURATION OF FEM SIMULATION

**Assembling Setup:** The assembling model consists of three parts: a  $30\text{ cm} \times 30\text{ cm}$  shell plane set as the deformable object, a  $40\text{ cm} \times 40\text{ cm} \times 4\text{ cm}$  rigid solid set as the tabletop, and two soft finger membranes. The target object is placed at the centre of the tabletop, with the sensors placed parallel to each other at a spacing of 80 cm, pressing onto the centre, edge, and corner of the paper, respectively.

**Property:** Here, we consider the deformable object as an office paper to simulate the grasping process. The material parameters of the paper based on the elastic model were set to *Mass Density*= $1.2e-9\text{ ton/mm}^3$ , *Young's Modulus*=828 MPa, *Poisson's Ratio*=0.3 [60]. The finger membrane was modelled using the Neo-Hookean hyperelastic model, with *Mass Density*= $1e-9\text{ ton/mm}^3$ ,  $C_{10}$ =0.0335,  $D_1$ =1.2297 [61].

**Step:** To replicate the actual dynamic contact process between the fingers and the paper, we chose the *Dynamic Explicit Analysis* method [62] and divided the interaction into two steps. In the first step, the finger presses the paper; in the second step, the finger grasps the paper through rotation, with

<sup>6</sup><https://www.gelsight.com/gelsightmini/>

each step lasting one second. The output measured is the total force due to the frictional stress between the fingers and the paper, allowing us to compare the magnitude of the frictional forces required at different contact locations.

**Interaction:** We have defined two types of contacts: the contact between the fingers and the paper; the contact between the paper and the tabletop. For both types, normal contacts and tangential contacts are defined. Tangential contact is defined using a penalty friction formulation, with the friction coefficients set as 0.5 and 0.1, respectively [63].

**Load:** The fingers will first execute a translational movement at a speed of 0.4 mm/s, pressing the paper in the direction perpendicular to the tabletop until the displacement reaches 0.4 mm. Then, the two fingers will rotate in opposite directions at a speed of 2 rad/s, twisting the paper from the table until the rotation angle reaches 2 radians. The tabletop remains fixed throughout the entire process.

## REFERENCES

- [1] C. Zhao, C. Jiang, J. Cai, M. Y. Wang, H. Yu, and Q. Chen, "Flipbot: Learning continuous paper flipping via coarse-to-fine exteroceptive-proprioceptive exploration," in *Proc. IEEE Int. Conf. Robot. Autom.*, 2023, pp. 10 282–10 288.
- [2] J. Zhu, A. Cherubini, C. Dune, D. Navarro-Alarcon, F. Alambeigi, D. Berenson, F. Ficuciello, K. Harada, J. Kober, X. Li *et al.*, "Challenges and outlook in robotic manipulation of deformable objects," *IEEE Robot. Autom. Mag.*, vol. 29, no. 3, pp. 67–77, 2022.
- [3] A. Billard and D. Kragic, "Trends and challenges in robot manipulation," *Science*, vol. 364, no. 6446, p. eaat8414, 2019.
- [4] C. B. Teeple, J. Werfel, and R. J. Wood, "Multi-dimensional compliance of soft grippers enables gentle interaction with thin, flexible objects," in *Proc. IEEE Int. Conf. Robot. Autom.*, 2022, pp. 728–734.
- [5] Y. Zheng, F. F. Veiga, J. Peters, and V. J. Santos, "Autonomous learning of page flipping movements via tactile feedback," *IEEE Trans. Robot.*, vol. 38, no. 5, pp. 2734–2749, 2022.
- [6] A. Koivikko, D.-M. Drotlef, C. B. Dayan, V. Sariola, and M. Sitti, "3d-printed pneumatically controlled soft suction cups for gripping fragile, small, and rough objects," *Adv. Intell. Syst.*, vol. 3, no. 9, p. 2100034, 2021.
- [7] L. Chin, F. Barscevicus, J. Lipton, and D. Rus, "Multiplexed manipulation: Versatile multimodal grasping via a hybrid soft gripper," in *Proc. IEEE Int. Conf. Robot. Autom.*, 2020, pp. 8949–8955.
- [8] C. Jiang, A. Nazir, G. Abbasnejad, and J. Seo, "Dynamic flex-and-flip manipulation of deformable linear objects," in *Proc. IEEE/RSJ Int. Conf. Intell. Robots Syst.*, 2019, pp. 3158–3163.
- [9] W. Yuan, S. Dong, and E. H. Adelson, "Gelsight: High-resolution robot tactile sensors for estimating geometry and force," *Sensors*, vol. 17, no. 12, p. 2762, 2017.
- [10] B. Ward-Cherrier, N. Pestell, L. Cramphorn, B. Winstone, M. E. Giannaccini, J. Rossiter, and N. F. Lepora, "The tactip family: Soft optical tactile sensors with 3d-printed biomimetic morphologies," *Soft Robot.*, vol. 5, no. 2, pp. 216–227, 2018.
- [11] C. Yang and N. F. Lepora, "Object exploration using vision and active touch," in *Proc. IEEE/RSJ Int. Conf. Intell. Robots Syst.*, 2017, pp. 6363–6370.
- [12] M. K. Johnson and E. H. Adelson, "Retrographic sensing for the measurement of surface texture and shape," in *Proc. IEEE Conf. Comput. Vis. Pattern Recognit.*, 2009, pp. 1070–1077.
- [13] I. H. Taylor, S. Dong, and A. Rodriguez, "Gelslim 3.0: High-resolution measurement of shape, force and slip in a compact tactile-sensing finger," in *Proc. IEEE Int. Conf. Robot. Autom.*, 2022, pp. 10 781–10 787.
- [14] M. Lambeta, P.-W. Chou, S. Tian, B. Yang, B. Maloon, V. R. Most, D. Stroud, R. Santos, A. Byagowi, G. Kammerer *et al.*, "Digit: A novel design for a low-cost compact high-resolution tactile sensor with application to in-hand manipulation," *IEEE Robot. Autom. Lett.*, vol. 5, no. 3, pp. 3838–3845, 2020.
- [15] S. Wang, Y. She, B. Romero, and E. Adelson, "Gelsight wedge: Measuring high-resolution 3d contact geometry with a compact robot finger," in *Proc. IEEE Int. Conf. Robot. Autom.*, 2021, pp. 6468–6475.
- [16] D. F. Gomes, Z. Lin, and S. Luo, "Geltip: A finger-shaped optical tactile sensor for robotic manipulation," in *Proc. IEEE/RSJ Int. Conf. Intell. Robots Syst.*, 2020, pp. 9903–9909.
- [17] A. Padmanabha, F. Ebert, S. Tian, R. Calandra, C. Finn, and S. Levine, "Ommitact: A multi-directional high-resolution touch sensor," in *Proc. IEEE Int. Conf. Robot. Autom.*, 2020, pp. 618–624.
- [18] H. Sun, K. J. Kuchenbecker, and G. Martius, "A soft thumb-sized vision-based sensor with accurate all-round force perception," *Nat. Mach. Intell.*, vol. 4, no. 2, pp. 135–145, 2022.
- [19] M. H. Tippur and E. H. Adelson, "Gelsight360: An omnidirectional camera-based tactile sensor for dexterous robotic manipulation," in *Proc. IEEE Int. Conf. Soft Robot.*, 2023, pp. 1–8.
- [20] G. Cao, J. Jiang, C. Lu, D. F. Gomes, and S. Luo, "Touchroller: A rolling optical tactile sensor for rapid assessment of textures for large surface areas," *Sensors*, vol. 23, no. 5, p. 2661, 2023.
- [21] W. Zhang, C. Xia, X. Zhu, H. Liu, and B. Liang, "Tactrot: A parallel-jaw gripper with rotatable tactile sensors for in-hand manipulation," in *Proc. IEEE Int. Conf. Syst. Man. Cybern.*, 2022, pp. 423–429.
- [22] S. Yuan, S. Wang, R. Patel, M. Tippur, C. Yako, E. Adelson, and K. Salisbury, "Tactile-reactive roller grasper," *arXiv preprint arXiv:2306.09946*, 2023.
- [23] S. Jin, C. Wang, and M. Tomizuka, "Robust deformation model approximation for robotic cable manipulation," in *Proc. IEEE/RSJ Int. Conf. Intell. Robots Syst.*, 2019, pp. 6586–6593.
- [24] Y. She, S. Wang, S. Dong, N. Sunil, A. Rodriguez, and E. Adelson, "Cable manipulation with a tactile-reactive gripper," *Int. J. Robot. Res.*, vol. 40, no. 12-14, pp. 1385–1401, 2021.
- [25] L. Pecyna, S. Dong, and S. Luo, "Visual-tactile multimodality for following deformable linear objects using reinforcement learning," in *Proc. IEEE/RSJ Int. Conf. Intell. Robots Syst.*, 2022, pp. 3987–3994.
- [26] A. Wilson, H. Jiang, W. Lian, and W. Yuan, "Cable routing and assembly using tactile-driven motion primitives," in *Proc. IEEE Int. Conf. Robot. Autom.*, 2023, pp. 10 408–10 414.
- [27] F. Zhang, A. Cully, and Y. Demiris, "Probabilistic real-time user posture tracking for personalized robot-assisted dressing," *IEEE Trans. Robot.*, vol. 35, no. 4, pp. 873–888, 2019.
- [28] R. Lee, D. Ward, V. Dasagi, A. Cosgun, J. Leitner, and P. Corke, "Learning arbitrary-goal fabric folding with one hour of real robot experience," in *Proc. Conf. Robot Learn.* PMLR, 2021, pp. 2317–2327.
- [29] N. Sunil, S. Wang, Y. She, E. Adelson, and A. R. Garcia, "Visuotactile affordances for cloth manipulation with local control," in *Proc. Conf. Robot Learn.* PMLR, 2023, pp. 1596–1606.
- [30] J. Zhu, M. Gienger, G. Franzese, and J. Kober, "Do You Need a Hand? – a Bimanual Robotic Dressing Assistance Scheme," *arXiv e-prints*, p. arXiv:2301.02749, Jan. 2023.
- [31] D. Navarro-Alarcon and Y.-H. Liu, "Fourier-based shape servoing: A new feedback method to actively deform soft objects into desired 2-d image contours," *IEEE Trans. Robot.*, vol. 34, no. 1, pp. 272–279, 2017.
- [32] S. Li, Z. Huang, T. Du, H. Su, J. B. Tenenbaum, and C. Gan, "Contact points discovery for soft-body manipulations with differentiable physics," *arXiv preprint arXiv:2205.02835*, 2022.
- [33] J. Zhu, B. Navarro, R. Passama, P. Fraise, A. Crosnier, and A. Cherubini, "Robotic manipulation planning for shaping deformable linear objects with environmental contacts," *IEEE Robot. Autom. Lett.*, vol. 5, no. 1, pp. 16–23, 2019.
- [34] Y. Qiu, J. Zhu, C. Della Santina, M. Gienger, and J. Kober, "Robotic fabric flattening with wrinkle direction detection," *arXiv preprint arXiv:2303.04909*, 2023.
- [35] K. Hang, A. S. Morgan, and A. M. Dollar, "Pre-grasp sliding manipulation of thin objects using soft, compliant, or underactuated hands," *IEEE Robot. Autom. Lett.*, vol. 4, no. 2, pp. 662–669, 2019.
- [36] V. Babin, D. St-Onge, and C. Gosselin, "Stable and repeatable grasping of flat objects on hard surfaces using passive and epicyclic mechanisms," *Robot. Comput. Integr. Manuf.*, vol. 55, pp. 1–10, 2019.
- [37] Q. Zhang, Z. Hu, K. Koyama, W. Wan, and K. Harada, "Prying grasp for picking thin object using thick fingertips," *IEEE Robot. Autom. Lett.*, vol. 7, no. 4, pp. 11 577–11 584, 2022.
- [38] T. Ko, "A tendon-driven robot gripper with passively switchable underactuated surface and its physics simulation based parameter optimization," *IEEE Robot. Autom. Lett.*, vol. 5, no. 4, pp. 5002–5009, 2020.
- [39] O. Azulay, N. Curtis, R. Sokolovsky, G. Levitski, D. Slomovik, G. Lilling, and A. Sintov, "Allsight: A low-cost and high-resolution round tactile sensor with zero-shot learning capability," *arXiv preprint arXiv:2307.02928*, 2023.

- [40] L.-C. Chen, Y. Zhu, G. Papandreou, F. Schroff, and H. Adam, “Encoder-decoder with atrous separable convolution for semantic image segmentation,” in *Proc. Eur. Conf. Comput. Vis.*, 2018, pp. 801–818.
- [41] F. Yu, V. Koltun, and T. Funkhouser, “Dilated residual networks,” in *Proc. IEEE Conf. Comput. Vis. Pattern Recognit.*, 2017, pp. 472–480.
- [42] K. He, X. Zhang, S. Ren, and J. Sun, “Deep residual learning for image recognition,” in *Proc. IEEE Conf. Comput. Vis. Pattern Recognit.*, 2016, pp. 770–778.
- [43] J. Jiang and S. Luo, “Robotic perception of object properties using tactile sensing,” in *Tactile Sensing, Skill Learning, and Robotic Dexterous Manipulation*. Elsevier, 2022, pp. 23–44.
- [44] R. Szeliski, *Computer vision: algorithms and applications*. Springer Nature, 2022.
- [45] R. Vidal, R. Tron, and R. Hartley, “Multiframe motion segmentation with missing data using powerfactorization and gpca,” *Int. J. Comput. Vis.*, vol. 79, pp. 85–105, 2008.
- [46] J. Zhang, M. Wu, and H. Dong, “Genpose: Generative category-level object pose estimation via diffusion models,” *Adv. Neural Inf. Process. Syst.*, 2023.
- [47] U. Asif, J. Tang, and S. Harrer, “EnsembleNet: Improving grasp detection using an ensemble of convolutional neural networks.” in *BMVC*, 2018, p. 10.
- [48] B. Audoly and Y. Pomeau, *Elasticity and geometry: from hair curls to the non-linear response of shells*. Oxford University Press, 2008.
- [49] I. E. Dzyaloshinskii, E. M. Lifshitz, and L. P. Pitaevskii, “The general theory of van der waals forces,” *Adv. Phys.*, vol. 10, no. 38, pp. 165–209, 1961.
- [50] Z. Lin, J. Zhuang, Y. Li, X. Wu, S. Luo, D. F. Gomes, F. Huang, and Z. Yang, “Gelfinger: A novel visual-tactile sensor with multi-angle tactile image stitching,” *IEEE Robot. Autom. Lett.*, 2023.
- [51] K. Shimonomura, T. Chang, and T. Murata, “Detection of foreign bodies in soft foods employing tactile image sensor,” *Front. Robot. AI.*, vol. 8, p. 774080, 2021.
- [52] R. Calandra, A. Owens, D. Jayaraman, J. Lin, W. Yuan, J. Malik, E. H. Adelson, and S. Levine, “More than a feeling: Learning to grasp and regrasp using vision and touch,” *IEEE Robot. Autom. Lett.*, vol. 3, no. 4, pp. 3300–3307, 2018.
- [53] R. Kalamuri, Z. Si, Y. Zhang, A. Agarwal, and W. Yuan, “Improving grasp stability with rotation measurement from tactile sensing,” in *Proc. IEEE/RSJ Int. Conf. Intell. Robots Syst.*, 2021, pp. 6809–6816.
- [54] W. Liang, F. Fang, C. Acar, W. Q. Toh, Y. Sun, Q. Xu, and Y. Wu, “Visuo-tactile feedback-based robot manipulation for object packing,” *IEEE Robot. Autom. Lett.*, vol. 8, no. 2, pp. 1151–1158, 2023.
- [55] F. R. Hogan, M. Bauza, O. Canal, E. Donlon, and A. Rodriguez, “Tactile regrasp: Grasp adjustments via simulated tactile transformations,” in *Proc. IEEE/RSJ Int. Conf. Intell. Robots Syst.*, 2018, pp. 2963–2970.
- [56] J. Jiang, G. Cao, A. Butterworth, T.-T. Do, and S. Luo, “Where shall i touch? vision-guided tactile poking for transparent object grasping,” *IEEE/ASME Trans. Mechatron.*, vol. 28, no. 1, pp. 233–244, 2022.
- [57] J. Lloyd and N. F. Lepora, “Goal-driven robotic pushing using tactile and proprioceptive feedback,” *IEEE Trans. Robot.*, vol. 38, no. 2, pp. 1201–1212, 2021.
- [58] —, “Pose-and-shear-based tactile servoing,” *Int. J. Robot. Res.*, 2023.
- [59] N. Funk, E. Helmut, G. Chalvatzaki, R. Calandra, and J. Peters, “Evetac: An event-based optical tactile sensor for robotic manipulation,” *arXiv preprint arXiv:2312.01236*, 2023.
- [60] M. Lee, S. Kim, H.-Y. Kim, and L. Mahadevan, “Bending and buckling of wet paper,” *Phys. Fluids*, vol. 28, no. 4, 2016.
- [61] C. Zhao, J. Ren, H. Yu, and D. Ma, “In-situ mechanical calibration for vision-based tactile sensors,” in *Proc. IEEE Int. Conf. Robot. Autom.*, 2023, pp. 10 387–10 393.
- [62] S. De, “Abaqus handout.”
- [63] L. Skedung, K. Danerlöv, U. Olofsson, C. M. Johannesson, M. Aikala, J. Kettle, M. Arvidsson, B. Berglund, and M. W. Rutland, “Tactile perception: Finger friction, surface roughness and perceived coarseness,” *Tribol. Int.*, vol. 44, no. 5, pp. 505–512, 2011.